AEDC-TR-66-97

Cy

SUMMARY OF IMPACT TESTING FOR NASA PROJECT SUPER

J. J. Payne
ARO, Inc.

September 1966

VON KÁRMÁN GAS DYNAMICS FACILITY
ARNOLD ENGINEERING DEVELOPMENT CENTER
AIR FORCE SYSTEMS COMMAND
ARNOLD AIR FORCE STATION, TENNESSEE

NOTICES

When U. S. Government drawings specifications, or other data are used for any purpose other than a definitely related Government procurement operation, the Government thereby incurs no responsibility nor any obligation whatsoever, and the fact that the Government may have formulated, furnished, or in any way supplied the said drawings, specifications, or other data, is not to be regarded by implication or otherwise, or in any manner licensing the holder or any other person or corporation, or conveying any rights or permission to manufacture, use, or sell any patented invention that may in any way be related thereto.

Qualified users may obtain copies of this report from the Defense Documentation Center.

References to named commercial products in this report are not to be considered in any sense as an endorsement of the product by the United States Air Force or the Government.

SUMMARY OF IMPACT TESTING FOR NASA PROJECT SUPER

J. J. Payne
ARO, Inc.

FOREWORD

The work reported herein was done at the request of the National Aeronautics and Space Administration (NASA), Marshall Space Flight Center (MSFC), under Project SUPER (Support Program for Extra-terrestrial Research), and performed under System 920E, Project 9514.

The results of tests presented were obtained by ARO, Inc. (a subsidiary of Sverdrup & Parcel and Associates, Inc.), contract operator of the Arnold Engineering Development Center (AEDC), Air Force Systems Command (AFSC), Arnold Air Force Station, Tennessee, under Contract AF40(600)-1200. The tests were conducted from February 5, 1965, through February 18, 1966, under ARO Project No. VS1443, and the manuscript was submitted for publication on April 13, 1966.

The author wishes to acknowledge the assistance of Mrs. Linda Welch for her work in the velocity and crater dimension determinations.

This technical report has been reviewed and is approved.

Donald E. Beitsch
Major, USAF
AF Representative, VKF
Directorate of Test

Leonard T. Glaser
Colonel, USAF
Director of Test

ABSTRACT

Hypervelocity impact tests were performed using Pegasus detector panels, simulated Saturn fuel tanks, and finite and semi-infinite targets. The impact velocity and crater parameters, where applicable, are given. It was determined that the output voltage of the Pegasus detector panels was not a function of projectile velocity nor of ambient pressure. The simulated Saturn fuel tanks showed evidence of burning after having been perforated by the projectile. The semi-infinite targets tested were 2024-T4, 6061-T6, and 7075-T6 Aluminum. Penetration data are presented for impact velocities from 11,000 to 30,300 fps and are used to determine values of target deformation stress. The correlation between the penetration data and an empirical relation using these stress values is approximately within ±2.5 percent. An empirical relationship to aid in crater volume prediction is presented. The results of the finite target work indicate that, to ensure that spall is not formed, the target thickness should be approximately 2.5 times the crater depth in a semi-infinite target.

CONTENTS

ILLUSTRATIONS

TABLES

NOMENCLATURE

D_c	Diameter of Crater
d_p	Diameter of projectile
P	Depth of penetration
S_t	Target deformation stress
T_o	Predicted depth of penetration in a semi-infinite target
T_T	Target thickness
V_c	Volume of crater
V_E	Velocity of ejecta
V_p	Velocity of projectile
V_s	Volume of spherical projectile
ρ_p	Projectile density
ρ_T	Target density

SECTION I
INTRODUCTION

This report is a summary of hypervelocity impact work performed for NASA. The work was accomplished in the Hypervelocity Impact Ranges (S-1) and (S-2) (Armament Test Cells, Hyperballistic (S1) and (S2)) of the von Kármán Gas Dynamics Facility (VKF).

The overall investigation is divided into four distinct efforts. They are:

1. To obtain the distributions of signal voltage resulting from impacting projectiles as functions of velocity and range pressure for the Pegasus impact detector panels.
2. To determine the resistance of a simulated Saturn fuel tank to hypervelocity impact, and to determine the reaction of this simulated tank to impact when filled with a life-supporting atmosphere.
3. To gather basic cratering data for semi-infinite targets of material useful for space vehicle applications.
4. To gather basic data from impacts into finite targets to supplement a theoretical program in which the elastic-plastic region of hypervelocity impact is to be treated.

SECTION II
PEGASUS DETECTOR PANELS

2.1 OBJECTIVE

The objective of the tests was to obtain distributions of signal voltage resulting from impacting projectiles as functions of velocity and range pressure.

2.2 TARGET DESCRIPTION

The detector tested (Fig. 1) was a flat plate capacitor, consisting of an aluminum (Al) target sheet 0.016 in. thick, a 0.5-mil Mylar® dielectric sheet, and a 0.000025-in.-thick vacuum-deposited layer of copper. The capacitor had a 2-in.-thick foam backing of polyurethane. This arrangement was attached to a frame made of a nonconducting material which provided adequate support against any possible overpressure resulting from the muzzle blast.

The test specimen was electrically connected in parallel with seven additional detectors. These detectors were to act as a load to simulate the electrical configuration used with the Pegasus, and were connected externally from the test tank by means of feed-through connectors. A power supply was connected to the test detector with the positive pole to the copper side. This power supply was used to place a 40-v potential across the test detector. The signal voltage was generated when the test detector was perforated.

2.3 PRIOR TESTING

The Pegasus meteoroid detection system was originally designed around a 10-v discriminator circuit; that is, any impact-induced signal of less than 10 v would not be relayed back to earth. Prior tests by others (Ref. 1) indicated that 50 percent of the signals produced by perforating projectiles were lower than 10 v and would therefore be rejected by the discriminator. Unfortunately, in these previous tests, the perforations ranged over a wide spectrum of hole sizes as well as projectile velocities, indicating that the test conditions were not closely controlled. The results of these tests were inconclusive, as it was impossible to be certain that the first signal seen from the detector resulted from a perforation. (There were many nonperforating impacts in addition to those causing perforation.)

2.4 TEST REQUIREMENTS

The results of the prior tests necessitated the requirement for controlled testing, that is, at a controlled velocity, known range pressure, and with impacts by projectiles relatively free of accompanying debris.

The test required 1/16-in.-diam projectiles (metallic and nonmetallic) to be launched at velocities ranging from 15,000 to 25,000 fps and at range pressures of 1 and 10 mm Hg. This portion of the program was done in Range S-2. This range and Range S-1, which was used in later portions of the test, are described in Appendix I.

2.5 INSTRUMENTATION

The primary velocity measurements were made with a high-speed framing camera. The 10-in. field of view of the camera included the target face and allowed both impact and pre-impact events to be recorded. A second method of obtaining velocity made use of two sheets

of aluminized plastic film located 17 ft apart. These sheets were perforated by the projectile and were used to produce electrical signals to start and stop a 10-mc chronograph. A more detailed description of these two systems is given in Ref. 2.

A secondary function of the high-speed framing camera was to detect the presence of debris and to determine whether the target was impacted first by debris or by the projectile. It was used to view the detector panel edge-on. The arrival of the projectile, traveling normal to the detector panel, was sensed by a sheet of aluminized plastic film which triggered the framing camera light source. The same aluminized plastic film also triggered an oscilloscope which monitored the output voltage from the detector.

2.6 RESULTS

The results of this series of firings are given in Table I. This table gives projectile material and velocity, detector output voltage, and range pressure. Useful results were obtained even from the firings in which the projectile failed to impact the target, in that there was an interest in knowing what effect, if any, the launcher operation (muzzle blast, vibration, electrical initiation) had on the target instrumentation. There was no noticeable effect on the target instrumentation from any of these firings where the projectile did not impact the target.

Graphic results of the tests are shown in Fig. 2, which is a plot of detector output voltage versus projectile velocity for range pressures of 1 and 10 mm Hg. This clearly does not indicate any correlation between output voltage and projectile velocity or output voltage and range pressure, although there appears to be a larger data spread at 10 mm than at 1 mm Hg. The tests did show, however, that the detector output generally was greater than 10 v (Table I), but in three cases output signals of less than 10 v were found. No operational peculiarities could be found to explain these low voltages, but in no case were they the result of nonperforating impacts.

As a result of the work reported herein, the following decisions were made by NASA: (1) the discriminator voltage level was reduced to 5 v on the Pegasus A prior to its launch; and (2) the discriminator voltage level was further reduced to 4 v on Pegasus B.

SECTION III
SATURN SPECIMENS

3.1 OBJECTIVE

The portion of the work described here was performed to aid in an evaluation of a man-rated orbital configuration. The areas to be investigated were (1) the resistance of the tank wall to meteoroid penetration, and (2) the reaction of the fuel tank, after being purged and filled with a life-supporting atmosphere, to meteoroid impact.

3.2 TARGET DESCRIPTION

The investigation involved two target configurations. These are illustrated in Fig. 3. The first, Fig. 3a, simulated a section of the booster wall and the second, Fig. 3b, simulated the pressurized fuel tank itself. The booster wall assembly (Fig. 3a) was an aluminum (Al) plate (0.117 in. thick) which had bonded to its rear face a 1-in.-thick, 6-in.-square piece of fiber glass reinforced polyurethane foam. A thin overcoat of epoxy covered the fiber glass portion of the assembly except as otherwise noted (Table II).

The fuel tank assembly (Fig. 3b) was essentially a 9-in.-long, 9-in.-OD cylinder with a plate similar to the wall structure at each end. Two front plate thicknesses were to be used in different parts of the test, one 0.063 in. thick and one 0.125 in. thick.

3.3 TEST REQUIREMENTS

The test required spherical 1/16- and 1/8-in.-diam projectiles to be launched into the specimens at velocities ranging from 12,000 to 27,000 fps. The range pressure to be used was 1 mm Hg. The test further required that the tank assembly be (1) impacted with the interior containing air at atmospheric pressure, (2) impacted with interior pressures of from 3.5 to 15 psia of both oxygen and nitrogen, and (3) impacted with an interior pressure of 7 psia of a 50-50 volumetric mixture of oxygen (O_2) and nitrogen (N_2).

3.4 INSTRUMENTATION

The high-speed framing camera, which was used to obtain projectile velocity,* was located with its optical axis normal to the flight

*The aluminized plastic film described earlier was used as an alternate velocity measuring system.

path of the projectile and such that the front face of both types of target specimens was in the field of view. The location of the camera with respect to the tank assembly is shown in Fig. 4. In the first few shots against the tank assembly (Fig. 3b), the film from this camera gave evidence of burning. To further investigate this a Fastax® framing camera was positioned to view the front face of the tank assembly during impact (Fig. 4). Later test conditions required a photographic view of the rear of the tank, and the camera was relocated. Both the locations are shown in Fig. 4.

The system used to obtain the desired atmosphere in the tank is shown in Fig. 4. The required gases were obtained from standard high-pressure bottles, and the required pressures were determined using a mercury manometer. The gas mixtures were obtained by pressurizing the target tank to half the desired pressure from the N_2 reservoir and then switching to the O_2 reservoir and pressurizing to the desired final pressure.

3.5 RESULTS

The results of the firings for this effort are given in Table II. Table IIa presents the results of the work involving the wall structures, and Table IIb presents the results of the work involving the tank assemblies. The velocities given, except where noted otherwise, were derived from data obtained using the high-speed framing camera system.

The remarks column of Table II describes the terminal effects of each launch. None of the wall specimens tested (Table IIa) were perforated, but the one impact by a 1/8-in.-diam projectile did break open the rear face. In all the tank firings (Table IIb), except the first two in which no foam was used, there were indications that the foam insulation had sustained minor burning. In order to determine the effect of tank volume on target burning, two identical tanks were bolted together end-to-end. The burning damage to two specimens in this configuration (shots SU-477 and 478, Table IIb) was noticeably greater than that sustained by the other specimens. This burning was further substantiated with the aid of the Fastax camera (Fig. 4) (framing rate - 7000 frames/sec). When the camera was used to monitor the front face of the target, burning was evident for durations of from 450 to 600 msec. The camera was moved to view the rear of the tank assembly (Fig. 4) midway in the test so that some insight into the nature of the burning inside the tank could be gained. In this position only three or four frames showed evidence of burning (nominally 0.5 msec).

Several overcoat materials were tried in order to eliminate the burning; as stated previously, all configurations tested showed signs of burning. The location of the overcoat is shown in Fig. 3b, and the overcoat materials are identified under the Remarks column of Table IIb.

SECTION IV
SEMI-INFINITE TARGETS

4.1 OBJECTIVE AND TEST REQUIREMENTS

This portion of the program was essentially a continuation of an earlier effort (reported in Ref. 2) to gather basic cratering data for semi-infinite targets of material useful for space vehicle application.

The tests required impacts of 1/8-in.-diam spherical projectiles into semi-infinite targets of 2024-T4, 6061-T6, and 7075-T6 Al. The projectiles used were 1100-0 Al, commercially pure titanium (Ti) and commercially pure magnesium (Mg). The experimental data required were projectile velocity and crater volume, diameter, and depth.

4.2 INSTRUMENTATION

The primary velocity measurements were made with a high-speed framing camera. Again, as mentioned previously, a second method of obtaining velocity made use of two sheets of aluminized plastic film located 45 ft apart.

4.3 TEST PROCEDURES

The target was mounted at the rear edge of the field of view of the framing camera and normal to the projectile line of flight. The target specimens were supported only at their edges, so that the rear faces were free of any encumberances. Throughout the entire test, none of the targets exhibited a distortion of the rear face.

4.4 DATA REDUCTION AND ACCURACIES

A complete description of the velocity data reduction technique using the high-speed framing camera is given in Ref. 2. When used as applied in the work reported here, velocity measurements made using this system are accurate within ±1 percent. The data reduction technique for the aluminized plastic film is straightforward, in that time

and distance are known, so velocity determination is a simple operation. The errors in the aluminized film velocity measuring system result from inaccuracy of measurements of the distance between the two stations and possible early penetration of the film by particles traveling at velocities greater than that of the projectile. A portion of this test was conducted without the benefit of the high-speed framing camera velocity measuring system, and the reported velocities are those derived from the aluminized film system alone. When velocity comparisons were made on those early shots in which both systems were used, nearly constant deviations of 10.56 percent (an average of 9 shots) were noted between measurements by the two methods. During later shots, deviations of ±0.25 percent were found. There was a distinct point in the conduct of this investigation beyond which the aluminized film method was improved and at which the averaged deviations of 10.56 percent ceased and those of ±0.25 percent started. Aluminized film velocities generated during the applicable portion of the test in which the high-speed framing camera was not used were therefore increased by 10.56 percent as a result of this analysis. These corrected velocities, when used, are properly noted.

The depths of the craters were measured to error limits of 0.3 percent by a technique described in Ref. 3. The volume measurements were made by metering a liquid filling agent into the craters. Use of a specially developed technique precludes volume measurement errors attributable to meniscus formation, and the measurements are accurate within 2-percent error limits. The effective diameter measurements were accomplished using a planimeter. The first step in determining this parameter is to mill the target lip off to the original target surface. A sheet of thin paper is then placed over the crater and a planimeter tracing is made around the perimeter of the crater. Two readings of this type are taken and the measured areas are averaged. The reported crater diameter is the diameter of a circle of equal area.

4.5 DISCUSSION AND RESULTS

Velocity and crater dimensions for all projectile-target combinations are given in Table III. The data in Table III are for the 2024-T4, 7075-T6, and 6061-T6 Al targets. Except where otherwise indicated, the velocity figures which appear in this table are those which resulted from the use of the framing camera.

4.5.1 Penetration Data

The penetration data, as presented in Figs. 5a and b, have been reduced to the form, P/d_p versus V_p, where penetration, P, is the distance from the original target surface to the bottom of the crater.

Following the same approach as that used in Ref. 2, the penetration data are correlated with the empirical prediction equation of Charters and Summers:

$$\frac{P}{d_p} = 0.5 \left(\frac{\rho_p}{\rho_T}\right)^{1/3} \left(\frac{\rho_p V_p^2}{2S_t}\right)^{1/3}$$

where S_t is assumed to be a constant deformation strength of the target material. Values of S_t were computed for a generous sampling of shots into 2024-T4 Al. These values are shown in Fig. 6, which is a plot of S_t versus projectile velocity. A mean S_t value of 1.25 emerged from Fig. 6. Using this value and the Charters-Summers relationship, the curves of Fig. 5a were established.

It is of interest to determine what influence variations in values of S_t have upon these empirically established curves. To evaluate this, the extremes of S_t shown in Fig. 6 (S_t = 1.18 and 1.48) were used to predict values of P/d_p. The resulting values of P/d_p showed average deviation of only 4 percent from those determined using a value of 1.25 for S_t (Fig. 5a). With this in mind, it appears that data from a single impact are sufficient to establish a value of S_t which will produce reasonable data correlation using the Charters-Summers relationship and the present data.

The S_t value for the 7075-T6 Al target material, thus determined, was then used to plot the empirical P/d_p versus V_p curve which appears in Fig. 5b. Also shown in Figs. 5a and b are the actual test points. Figures 5a and b show very good agreement between the actual and the predicted penetration ratios. The percentage of variation between the actual and the predicted P/d_p ratios for each shot for the 2024-T4, 7075-T6, and 6061-T6 Al is given in Table III. These percentage variations are based on the empirically predicted ratios. Neglecting two shots (SU-370 and SU-372) the averaged deviations for the 2024-T4 Al are +2.33 and -2.58 percent. The averaged positive deviation for the 7075-T6 Al is 1.8 percent. Only two shots of this series indicated a penetration ratio less than was predicted, so nothing can be said about any negative deviation for the 7075-T6 Al.

There are not enough data on the 6061-T6 Al targets to make any analysis meaningful. The crater parameter data are included in the latter portion of Table III, and it is obvious from the percentage deviations of the actual from the predicted penetration ratios that these data are useless as far as evaluating them in terms of P/d_p versus V_p. No explanation can be offered for the large variations in these data. All measurement techniques used in the 6061-T6 Al tests were exactly the same as those used for the 2024-T4 and the 7075-T6 Al.

For the tests described herein, the values of S_t calculated using the Charters-Summers relationship are:

$$\text{2024-T4 Al:} \quad 1.250 \frac{\text{gm-km}^2}{\text{cc-sec}^2}$$

$$\text{7075-T6 Al:} \quad 1.315 \frac{\text{gm-km}^2}{\text{cc-sec}^2}$$

For the purpose of coherence, the values of S_t obtained during the work described in Ref. 2 are repeated; they are:

$$\text{304 Stainless Steel:} \quad 1.899 \frac{\text{gm-km}^2}{\text{cc-sec}^2}$$

$$\text{2024-0 Al:} \quad 0.6016 \frac{\text{gm-km}^2}{\text{cc-sec}^2}$$

$$\text{1100-0 Al:} \quad 0.3425 \frac{\text{gm-km}^2}{\text{cc-sec}^2}$$

The apparent inconsistency between the values of S_t and the materials used can be explained when the Brinell hardness of each material is compared with its corresponding value of S_t; they are:

Target Material	Brinell Hardness (Ref. 4)	S_t
1100-0 Al	23	0.3425
2024-0 Al	47	0.6016
2024-T4 Al	120	1.250
7075-T6 Al	150	1.315

The most obvious conclusion to be drawn from this is that S_t has a dependence on the Brinell hardness of the target material. This dependence is further substantiated by Fig. 7 which is a plot of Brinell hardness versus S_t. This clearly shows S_t to be a nearly linear function of Brinell hardness, at least for these aluminum alloys and over the range that has been investigated.

In order to evaluate the validity of the penetration prediction equation further, other sources of data were investigated. Figure 8 is a plot of P/d_p versus V_p, again for 2024-T4 Al, following Ref. 5. This plot was made independently of the data discussed earlier, and it is interesting to note that the value of S_t is the same as that derived from the data generated during this study (1.25). Figure 8 further shows, as is implied and expected, that the equation is independent of projectile diameter, at least for the range of diameters shown.

The credence to be given the equation is further increased in consideration of the high purity copper target work of Liles and Goodman (Ref. 6). Figure 9 is a plot of P/d_p versus V_p for impacts into these targets. There appears to be very reasonable agreement between the experimental data and the prediction curve. The difference between the actual and the predicted penetration appears to be almost the same as that in Ref. 2. The value of S_t calculated using the Charters-Summers relationship for this work is 0.740 gm-km^2/cc-sec^2.

Still more P/d_p data for 1100-0 Al are shown in Fig. 10. Some of these data were generated in VKF under separate tests, but most came from Ref. 6 (Al on Al and Cu on Al). The lead (ρ_p = 11.0) and copper (ρ_p = 8.77) points, though few in number, show the validity of taking a previously determined value of S_t and predicting a P/d_p ratio for a given projectile material impact. The Al on Al curve (ρ_p = 2.7) shows very good agreement between the actual and predicted values along the higher portion of the curve, but a certain disagreement exists on the lower portion (10,000 to 14,000 fps). The velocity and crater parameter data for the points not drawn from the references which are indicated on Fig. 10 are given in Table IV. Except where otherwise indicated, the velocity figures which appear in Table IV were derived by the use of the framing camera.

4.5.2 Crater Diameter

Figure 11 is a plot of crater diameter as a function of projectile velocity for titanium and magnesium impacts into 2024-T4 and 7075-T6 Al (Table III). Within the limitations of these data, and for the other data presented in this report, the crater diameter is a linear function of the projectile velocity. The main purpose of Fig. 11 is not to document the above stated conclusion, which is well known, but to explain the scatter of the data. It is obvious from a comparison of Figs. 11 and 5a (the penetration data), that the data spread is larger on Fig. 11 for the crater diameters.

Impacts into brittle targets (such as 2024-T4, 7075-T6, and 6061-T6 Al) do not yield the type of crater lip that is common on impacts into ductile target materials. The impacts into brittle targets cause severe fracturing of the area around the lip. The technique used to measure crater diameters for these specimens is described in Section 4.4 of this report. Figure 12 is a photograph of a 7075-T6 Al target prepared for crater diameter measurement. It is obvious upon examination that the crater periphery is very irregular. With irregularities as shown in Fig. 12, the crater diameter data at best are not going to have the orderliness that can be expected from data derived from more ductile targets wherein crater cross sections are more nearly circular.

4.5.3 Crater Volume

A portion of the crater volume data generated during this program is presented in Fig. 13, and a portion from Ref. 2 is presented in Fig. 14. These are plots of the dimensionless ratio V_c/V_s (crater volume/spherical projectile volume) versus projectile velocity. The curve V_c/V_s shown was derived from an empirical relationship of the form used in Refs. 6 and 7, but with changed coefficient and exponents, viz,

$$V_c/V_s = 0.57\,(\rho_p/\rho_T)^{0.25}\left(\frac{\rho_p V_p^2}{2S_t}\right)^{0.95}$$

The values of the constant (0.57) and the exponents (0.25 and 0.95) were derived by a solution of three equations with three unknowns, of the type

$$V_c/V_s = K\,(\rho_p/\rho_T)^X\left(\frac{\rho_p V_p^2}{2S_t}\right)^Y$$

and the values presented are averages from several such operations.

Figures 13 and 14 show reasonable agreement between the prediction curves and the experimental points. The agreement, although reasonable, is not quite as good as in the case of the penetration data (Figs. 5, 8, 9, and 10), but appears to be about as good as shown for the crater diameter data. The explanation given for the variation in the crater diameter (crater lip irregularities, Fig. 12) is one possible source of variation in the V_c/V_s data, since randomness in volume measurements is related to randomness in diameter measurements. The agreement might be bettered considerably if a very large amount of data were used in the determination of the constant and the exponents given in the above relationship. Within the scope of the data presented in this report, the above relationship seems to adequately describe the dependence of the crater volume on the variables given.

SECTION V
FINITE TARGET STUDY

5.1 OBJECTIVE AND REQUIREMENTS

This portion of the work was to supplement a theoretical program in which the elastic-plastic behavior of hypervelocity impact is to be treated and in which spall and perforation threshold velocities are of particular interest.

The tests required impacts of 1/16-, 1/8-, 3/16-, and 1/4-in.-diam spherical Al projectiles into various thicknesses of 6061-T6 Al targets. These launchings were to be performed at 1-mm Hg range pressure. Specifically, the shots to be fired were:

(1) 1/16-in. into targets of thicknesses 1.0 T_o; 1.5 T_o; 2.0 T_o; 2.5 T_o; 3.0 T_o; 4.0 T_o and 5.0 T_o

(2) same for 1/8-in.

(3) same for 3/16-in.

(4) same for 1/4-in.

where T_o is the predicted depth of penetration in a semi-infinite target. The experimental data required were projectile velocity; crater volume, diameter, and depth; and, in cases where spall or perforation was expected, the spall or perforation velocity.

5.2 INSTRUMENTATION

The velocity measurement techniques used in this portion of the program were the same as those described in Section II, i.e., high-speed framing camera and aluminized plastic film.

5.3 TEST PROCEDURES

The target specimens were mounted in the center of the field of view of the framing camera and normal to the projectile line of flight. This arrangement allowed both projectile velocity and the spall and ejecta velocities to be determined. The test specimens were supported only at their edges, so that the rear faces were free of any encumberances.

5.4 DATA REDUCTION AND ACCURACIES

The data reduction techniques and their corresponding accuracies as described earlier are also applicable to this portion of the program.

5.5 DISCUSSION AND RESULTS

Velocity, crater dimensions, and target thickness for all projectile target combinations are given in Table V. Except where otherwise indicated, the velocity figures which appear in this table are those which resulted from the use of the framing camera.

The discussion of the results of this portion of the test will not deal with the elastic-plastic region of hypervelocity impact but with the more straightforward aspects of impact.

5.5.1 Penetration

Figure 15 is a series of plots of penetration (P) versus target thickness (T_T) for impacts of 1/4-, 3/16-, and 1/8-in.-diam projectiles. These plots show a decreasing penetration as the target thickness is increased, as is to be expected since the thicker target offers more resistance to deformation. These results are in agreement with those published in Ref. 9. Figure 15 further shows that at some point (depending on projectile diameter) the target thickness ceases to be a determining factor in the final crater depth, for nominally constant projectile velocities.

Many authors have stated that target thicknesses (T_T) should be 1.5 times the crater depth in a semi-infinite target to prevent either perforation or spall (the ejection of material from the back of the target) (Ref. 8). Using this factor of 1.5 and the previously discussed penetration relationship, the required target thickness to prevent either perforation or spall for this material should be:

for 1/8-in.-diam Al projectile - 0.35 in.

for 3/16-in.-diam Al projectile - 0.53 in.

for 1/4-in.-diam Al projectile - 0.71 in.

These values were computed for V_p = 24,000 fps and S_t = 1.308. Table VI is a tabulation of the terminal effects of this series of firings, and it gives projectile velocity and diameter, target thickness to penetration ratio, and remarks as to whether the target was perforated, spalled, deformed, or suffered no effect. The results in Table VI show that spall was formed at the following maximum target thicknesses:

for 1/8-in.-diam projectile - 0.47 in.

for 3/16-in.-diam projectile - 0.89 in.

for 1/4-in.-diam projectile - 0.95 in.

All of these plates were considerably thicker than those based on the 1.5-times-the-crater-depth rule, and yet spall was formed. It appears that the value of 1.5 is too low, and, based on the results of these tests, to ensure that spall is not formed, the target should be approximately 2.5 times the crater depth in a semi-infinite target. This value of 2.5 is based on the results in Table VI, wherein targets whose thickness was approximately 2 times the expected crater depth in a semi-infinite target

spalled, and those with thicknesses of approximately 2.5 times the expected crater depth in a semi-infinite target failed to spall.

Figure 16 is a photograph of typical results obtained from this test. These plates, ranging in thickness from 0.475 to 1.800 in. were impacted by 1/4-in.-diam 2017 Al spheres. This figure vividly illustrates what is meant by spall (the bottom side of the first three plates) and further shows that the remainder of the plates were deformed by the impact. The bottom plate (1.8 in. thick) illustrates what is meant in Table VI by very slight rear surface deformation. When examined closely, it can be seen that a slight fracture had commenced.

5.5.2 Ejecta Velocities

The ejecta (the material ejected uprange from the front face of the target) velocities (V_E) obtained during the course of the test are given in Table VII. The most interesting point of this aspect of the work is that the ejecta velocities were all lower than the projectile velocity. The highest ejecta velocities were approximately 23 percent lower than those of the projectile. Within the very limited scope of these data, this appears to be in disagreement with previous information that ejecta velocities 8 to 10 times that of the projectile can be expected (Ref. 9).

Figure 17 is a plot of the dimensionless ratio, projectile velocity per ejecta velocity (V_p/V_E), versus target thickness. This graph shows that the ejecta velocity decreases with increasing target thickness. It would appear that the intensity of the shock wave within the target (after reflection from the rear to the front face) plays a significant role in the ejecta velocity. The thicker the target, the weaker the shock intensity upon reflection to the front face of the target, perhaps lowering the ejecta velocity; conversely, the thinner target produces a stronger reflected shock at the front face of the target which may cause the evident increase of ejecta velocity.

SECTION VI
MISCELLANEOUS LAUNCHINGS

A limited number of ad hoc firings were made on special request. These firings were out of the normal routine of testing, and no analytical work has been performed with the data. Table VIII lists all the firings of this type along with all pertinent data.

The reason for the impacts into the Norbide® targets was simply to determine the reaction of the material to hypervelocity impact. The targets, in all cases, fractured into small pieces.

The launches of the Dylite® spheres were made to determine if projectiles of very low densities (0.035 gm/cc, in this case) could be launched from light-gas guns. This work was in preparation for future impact testing similar to that described earlier in regard to the Pegasus detector panel (Section II).

REFERENCES

1. Private Communicaion with R. J. Naumann, NASA, Marshall Space Flight Center, March 3, 1966.
2. Payne, J. J. "Impacts of Spherical Projectiles of Aluminum, Stainless Steel, Titanium, Magnesium, and Lead into Semi-Infinite Targets of Aluminum and Stainless Steel." AEDC-TR-65-34 (AD456391), February 1965.
3. Goodman, E. H. "Description of Terminal Ballistic Ranges." AEDC-TDR-62-104 (AD275362), May 1962.
4. Reynolds Aluminum Data Book. Reynolds Metal Company, 1958, p. 91.
5. Denardo, B. Pat, and Nysmith, C. Robert. "Momentum Transfer and Cratering Phenomena Associated with the Impact of Aluminum Spheres into Thick Aluminum Targets at Velocities to 24,000 Feet Per Second." NASA-TMX54, 046.
6. Liles, C. D. and Goodman, E. H. "Particle Solid Impact Phenomena." AEDC-TR-62-202 (AD287808), November 1962.
7. Bruce, E. P. "Review and Analysis of High Velocity Impact Data." Proceedings of the Fifth Symposium on Hypervelocity Impact, p. 439.
8. Christman, D. R., Gehring, J. W., Maiden, C. J., and Wenzel, A. B. "Study of the Phenomena of Hypervelocity Impact." GM-DRL-TR-63-216, June 1963.
9. Kinslow, Ray. "Properties of Spherical Stress Waves Produced by Hypervelocity Impact." AEDC-TDR-63-197 (AD421578), October 1963.

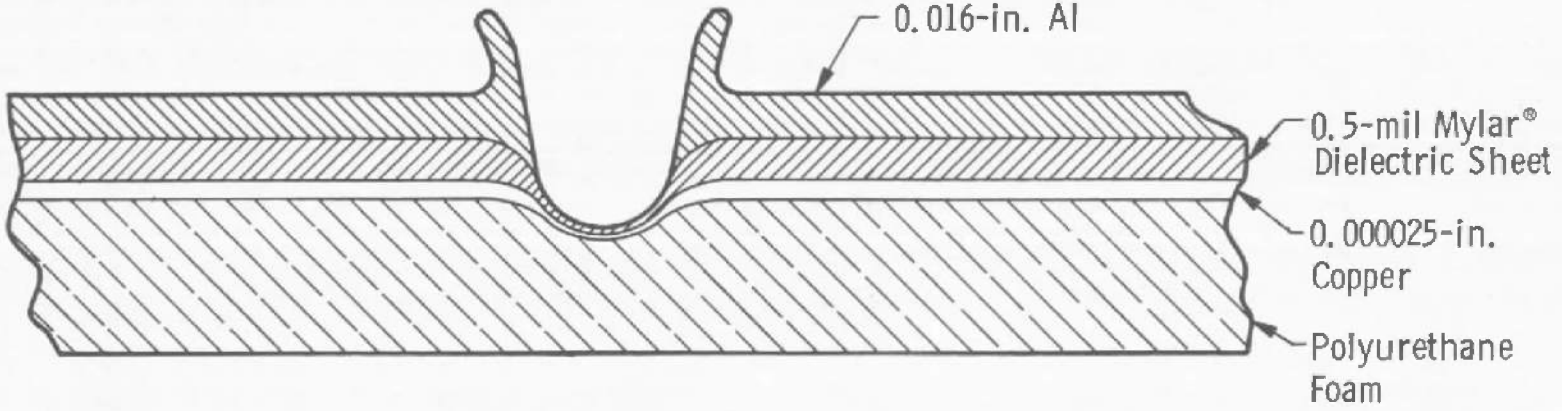

Fig. 1 Sectioned View of Impacted Pegasus Detector Panel

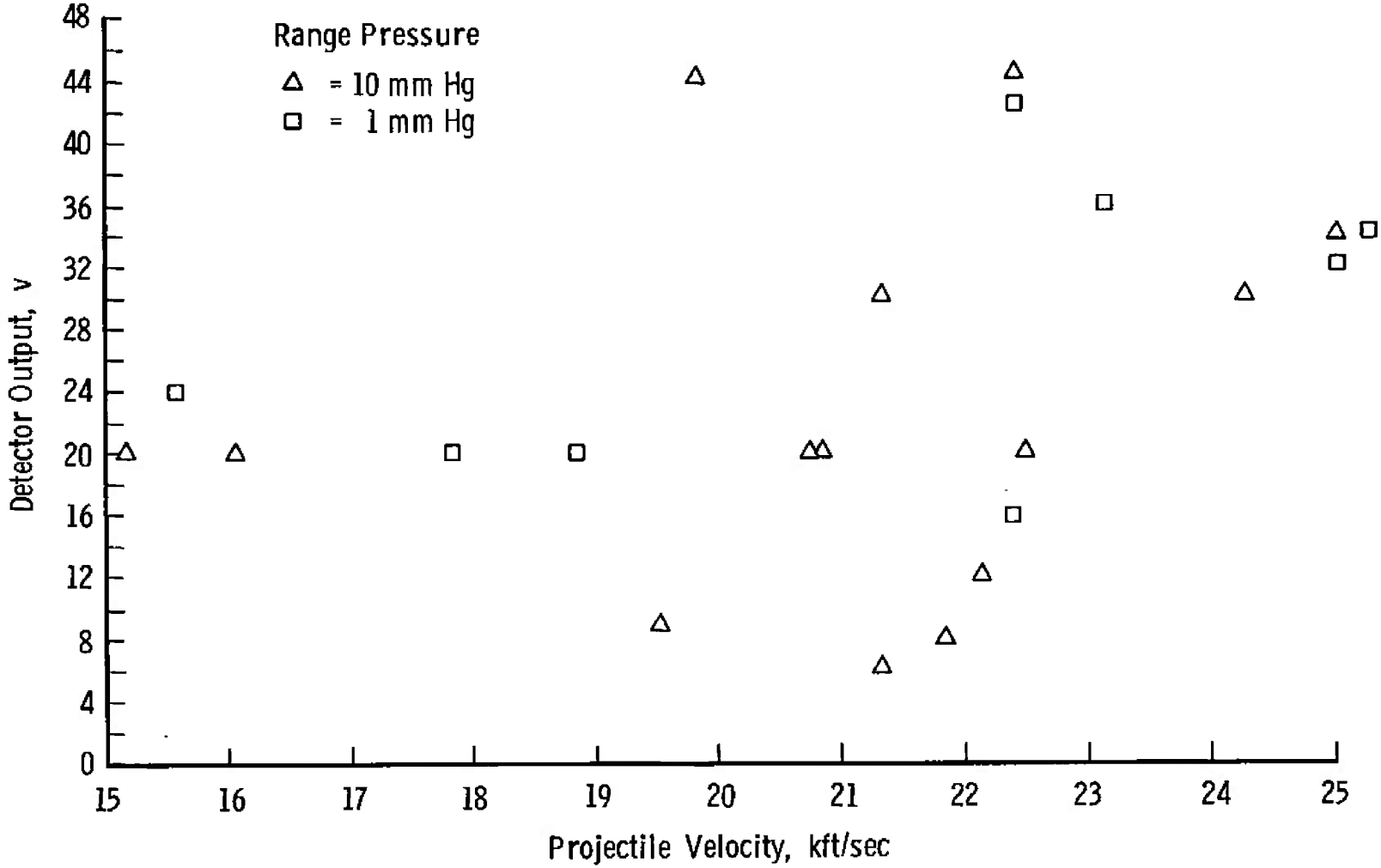

Fig. 2 Detector Output versus Projectile Velocity

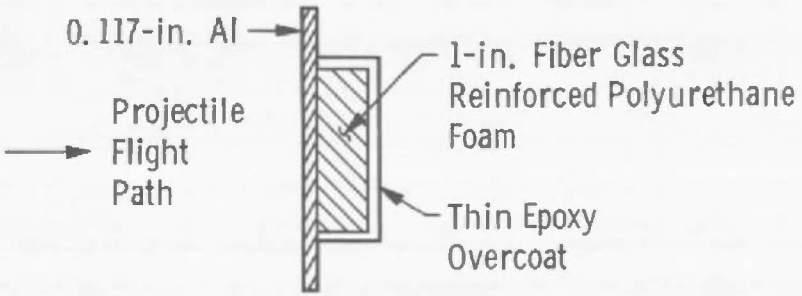

a. Saturn Wall Assembly

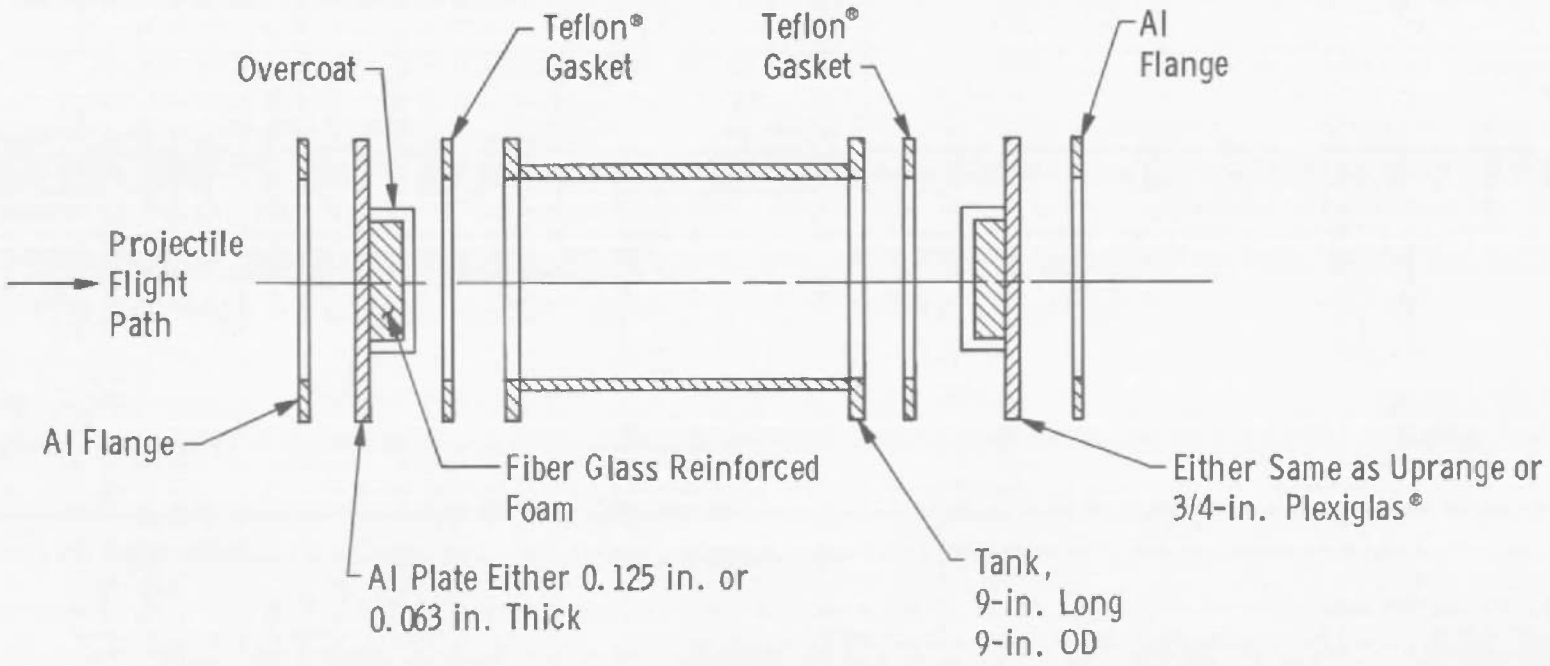

b. Saturn Tank Assembly

Fig. 3 Saturn Target Configurations

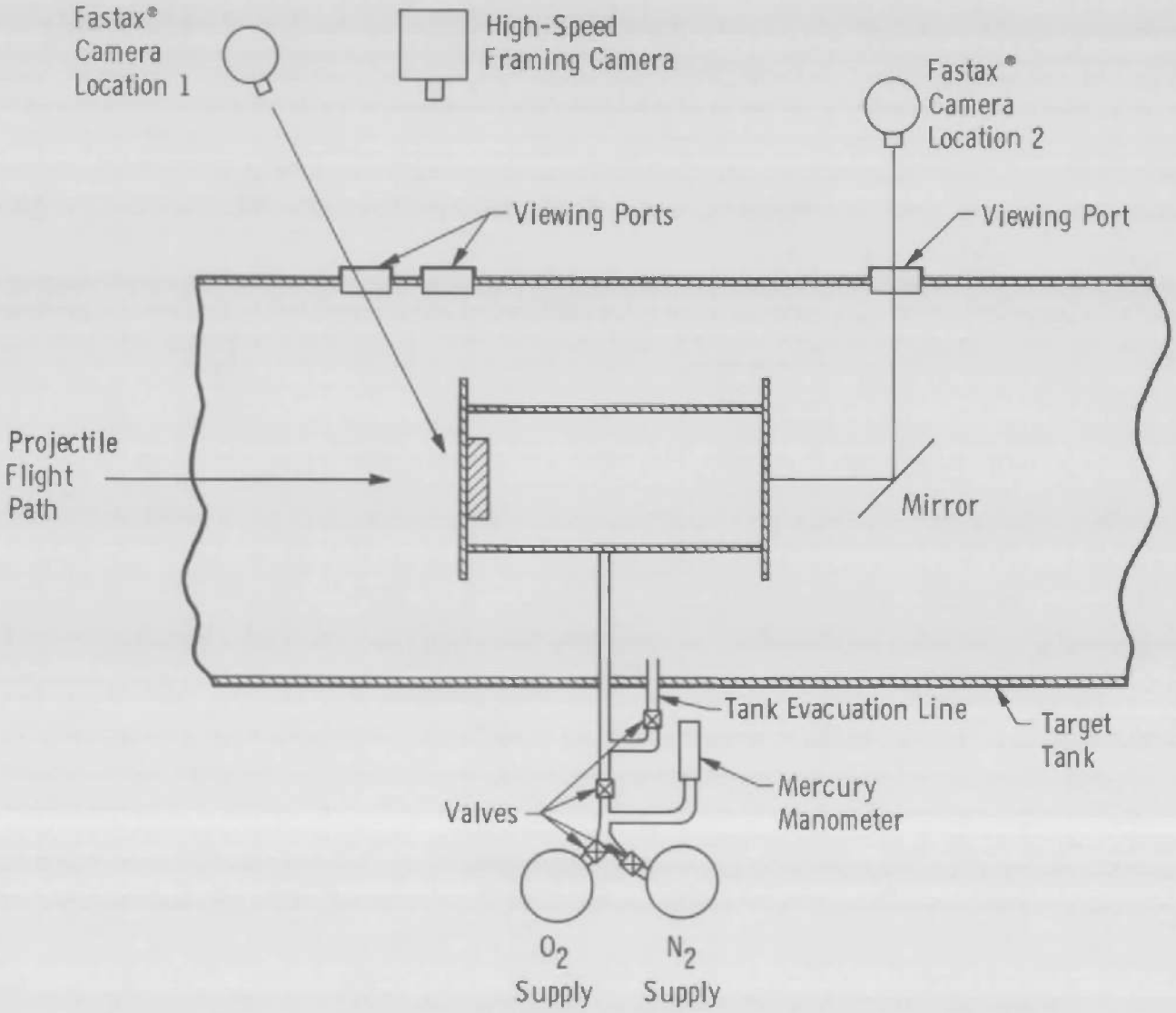

Fig. 4 Photographic and Pressuration System for Saturn Tank

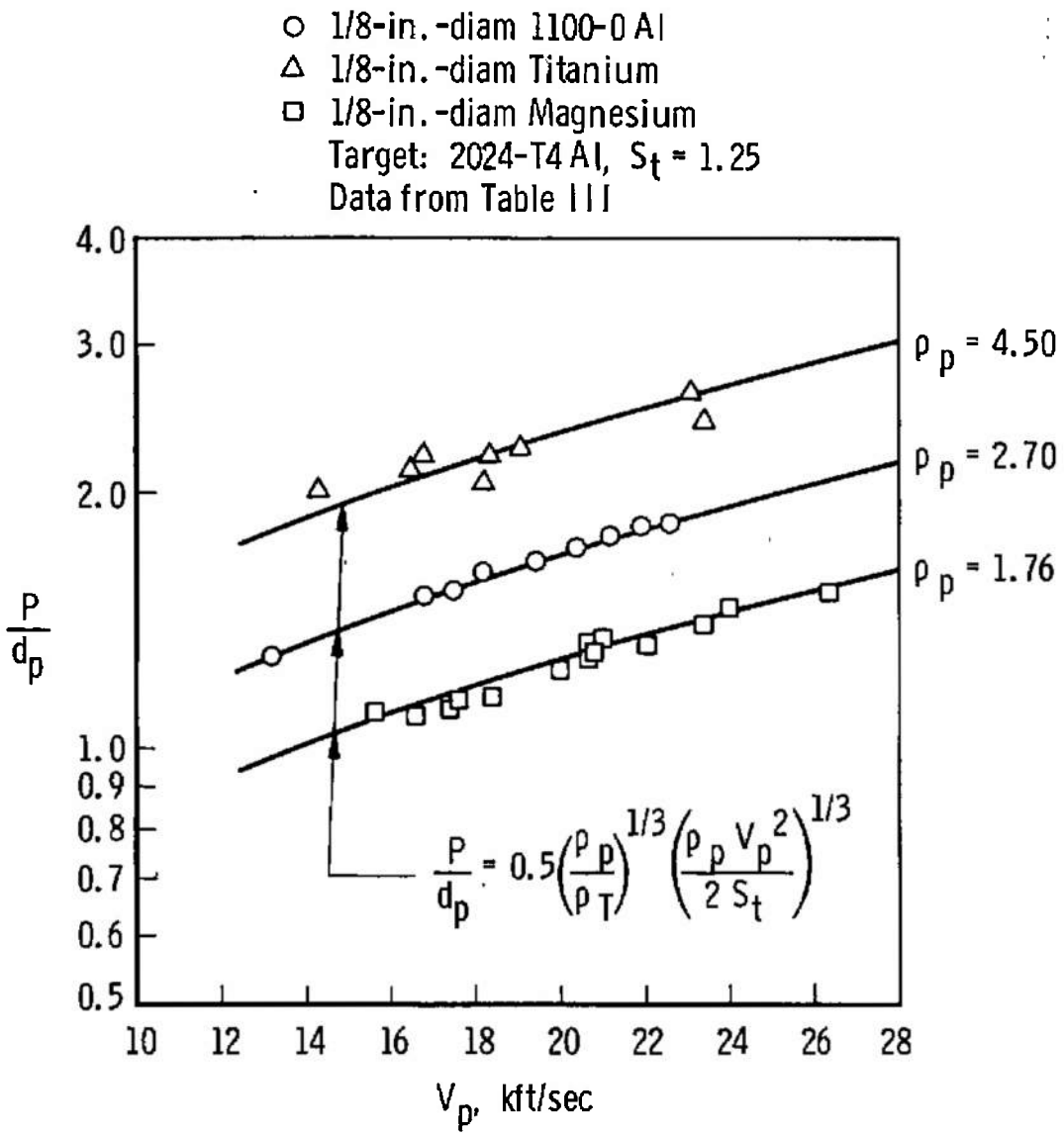

a. 2024-T4 Targets

Fig. 5 Data Correlation for Aluminum Targets

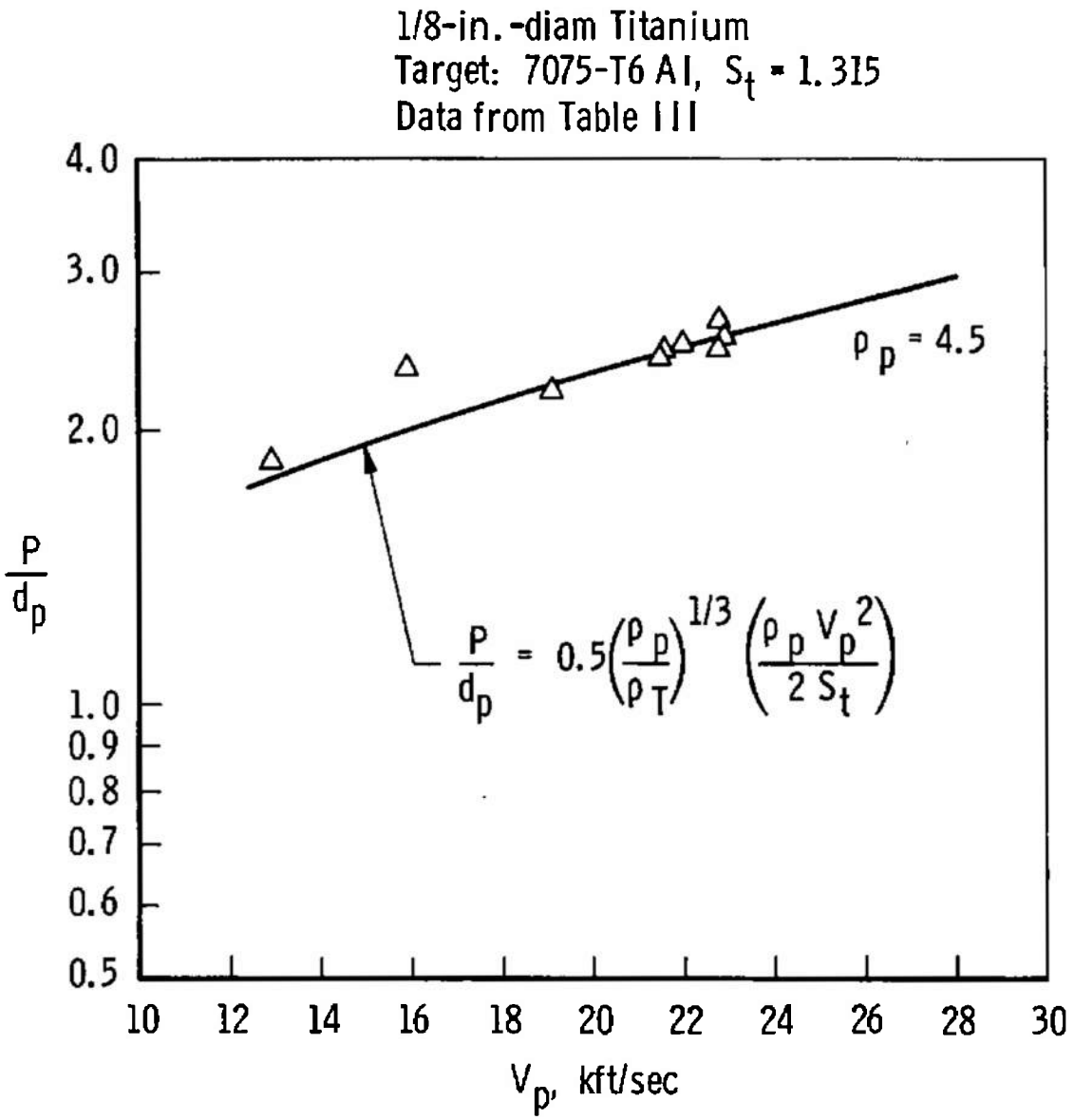

b. 7075-T6 Targets

Fig. 5 Concluded

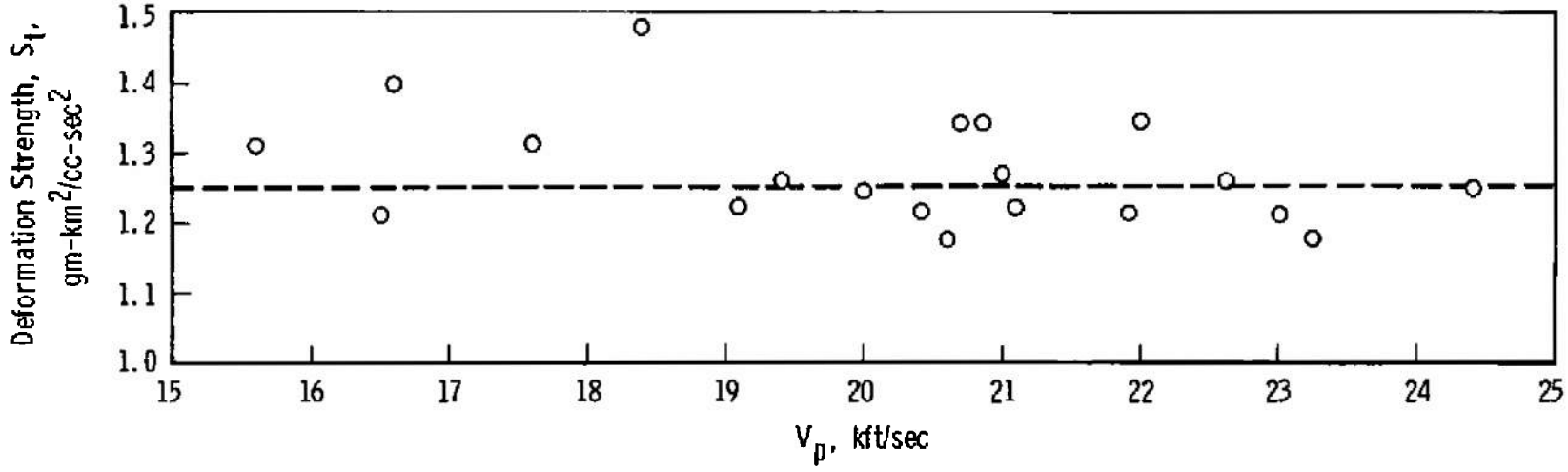

Fig. 6 Deformation Stress versus Projectile Velocity

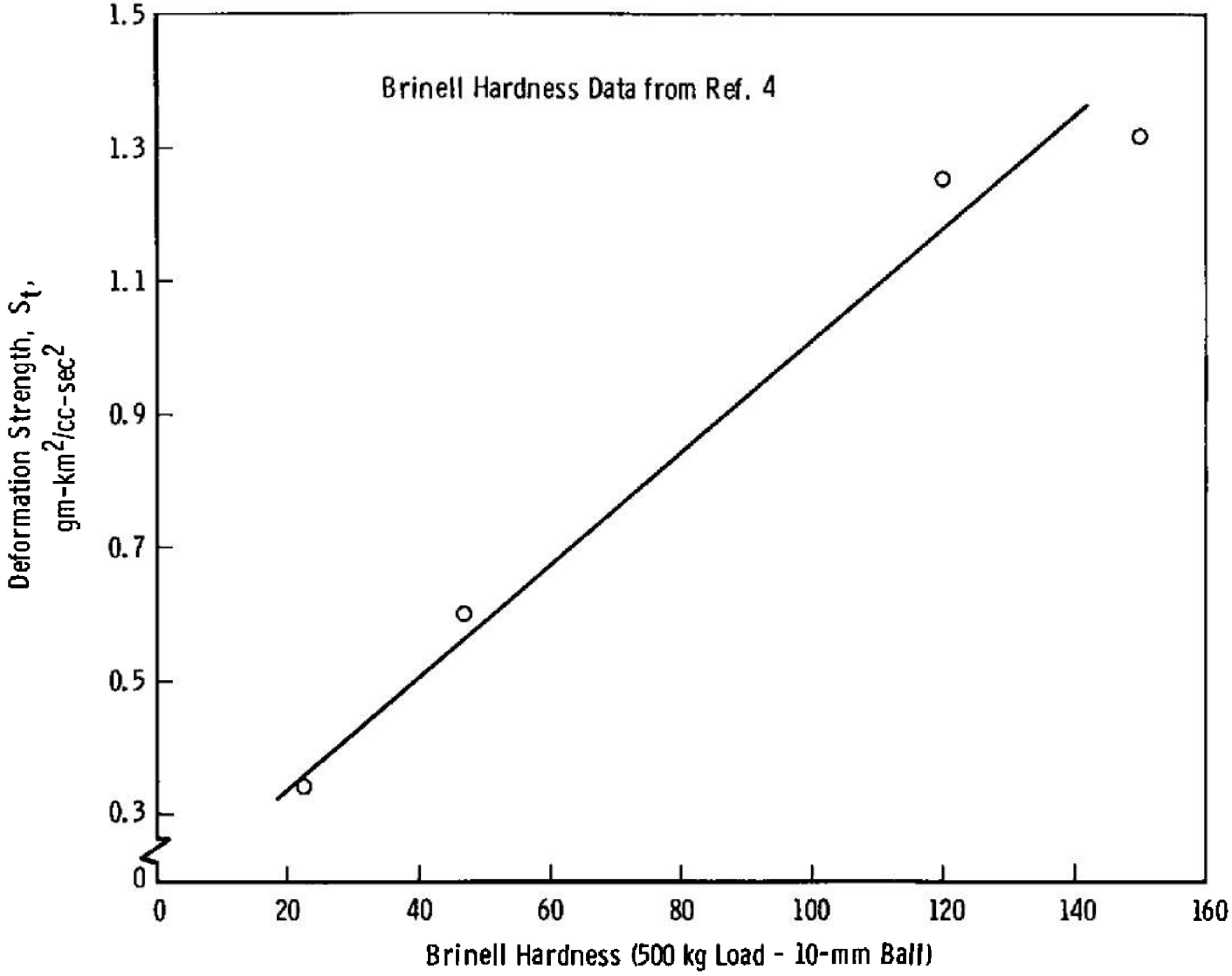

Fig. 7 Brinell Hardness versus Deformation Stress

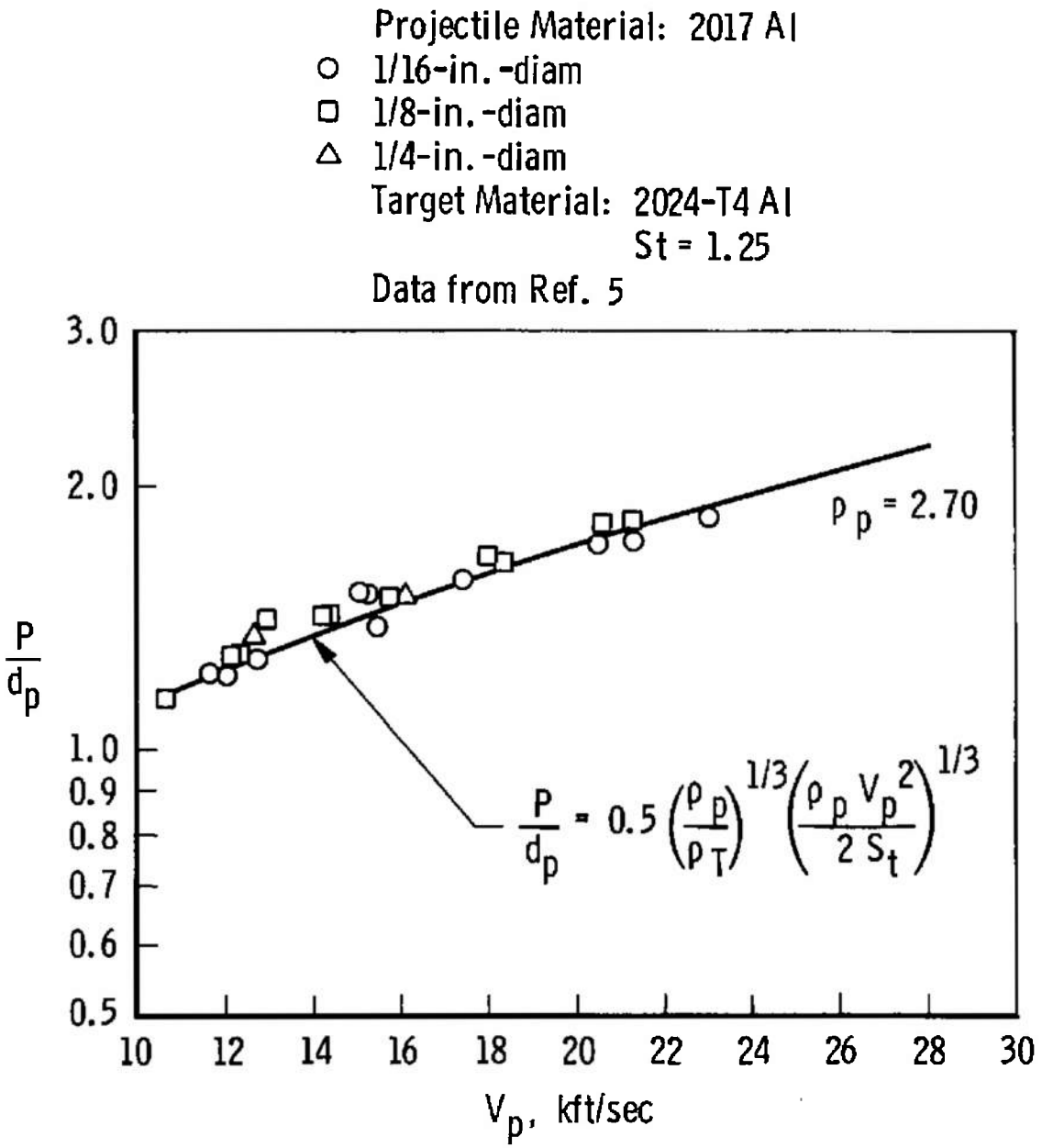

Fig. 8 Correlation of NASA Data for 2024-T4 Al Targets

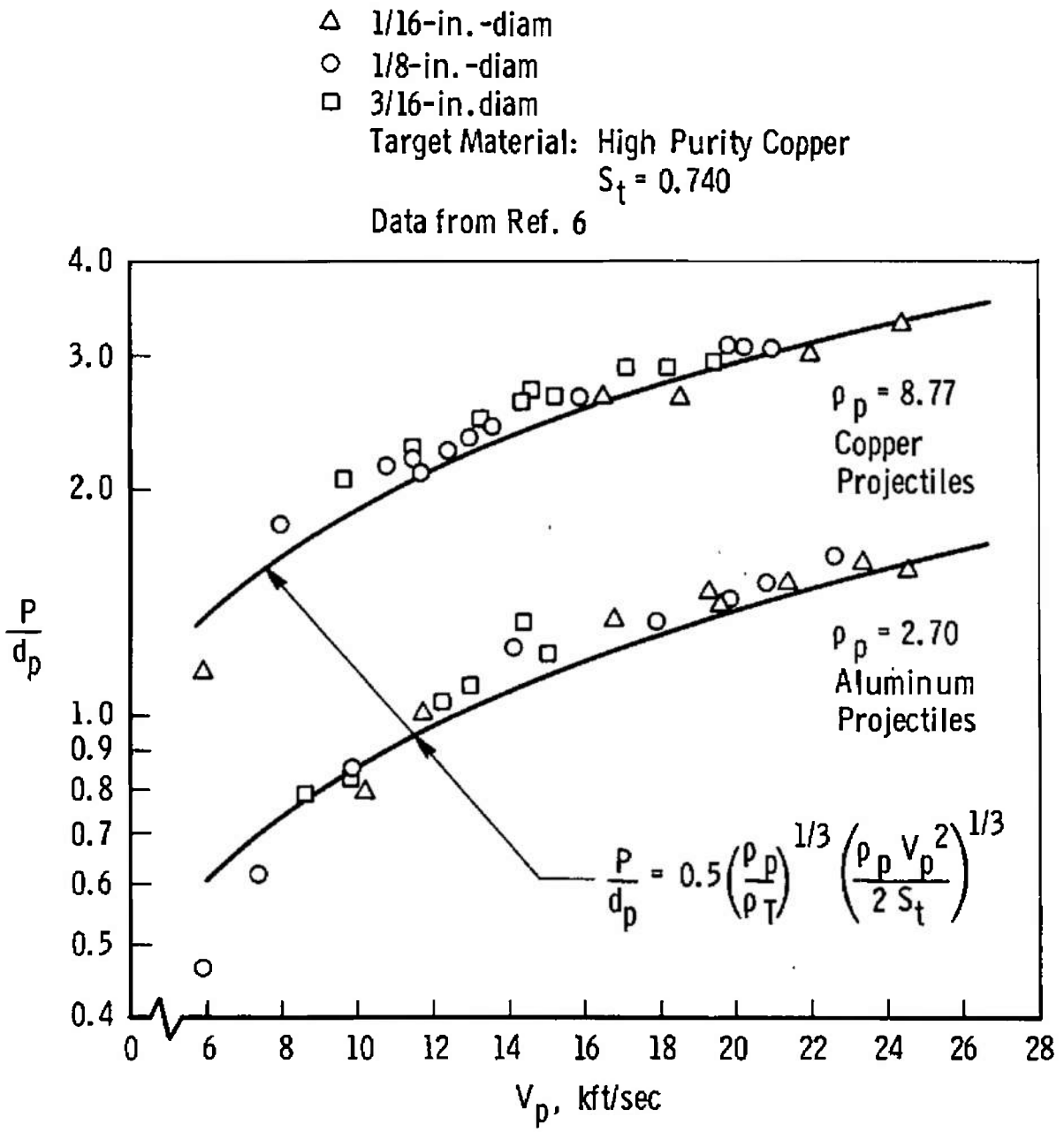

Fig. 9 Data Correlation for Copper Targets

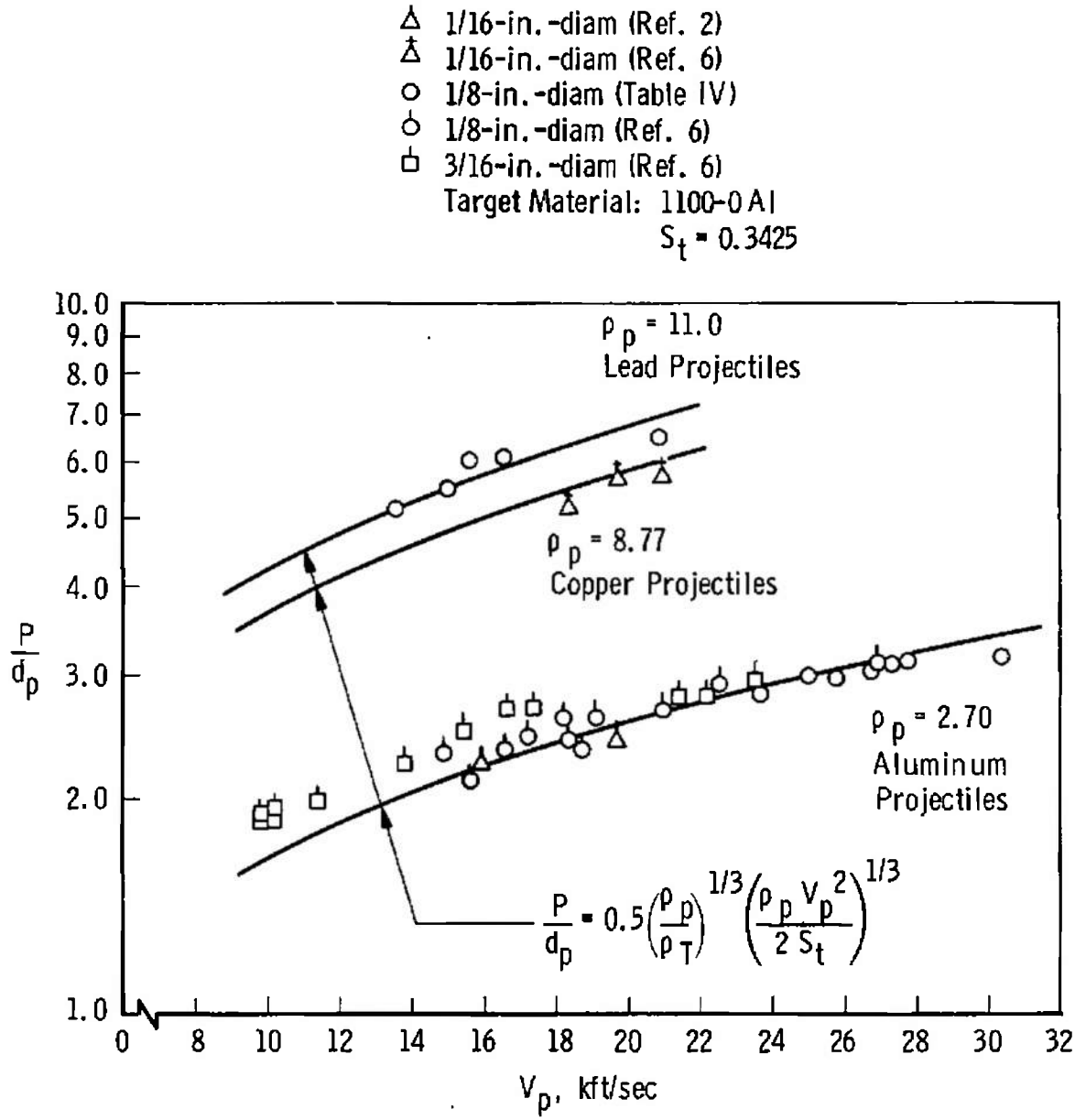

Fig. 10 Data Correlation for 1100-0 Al Targets

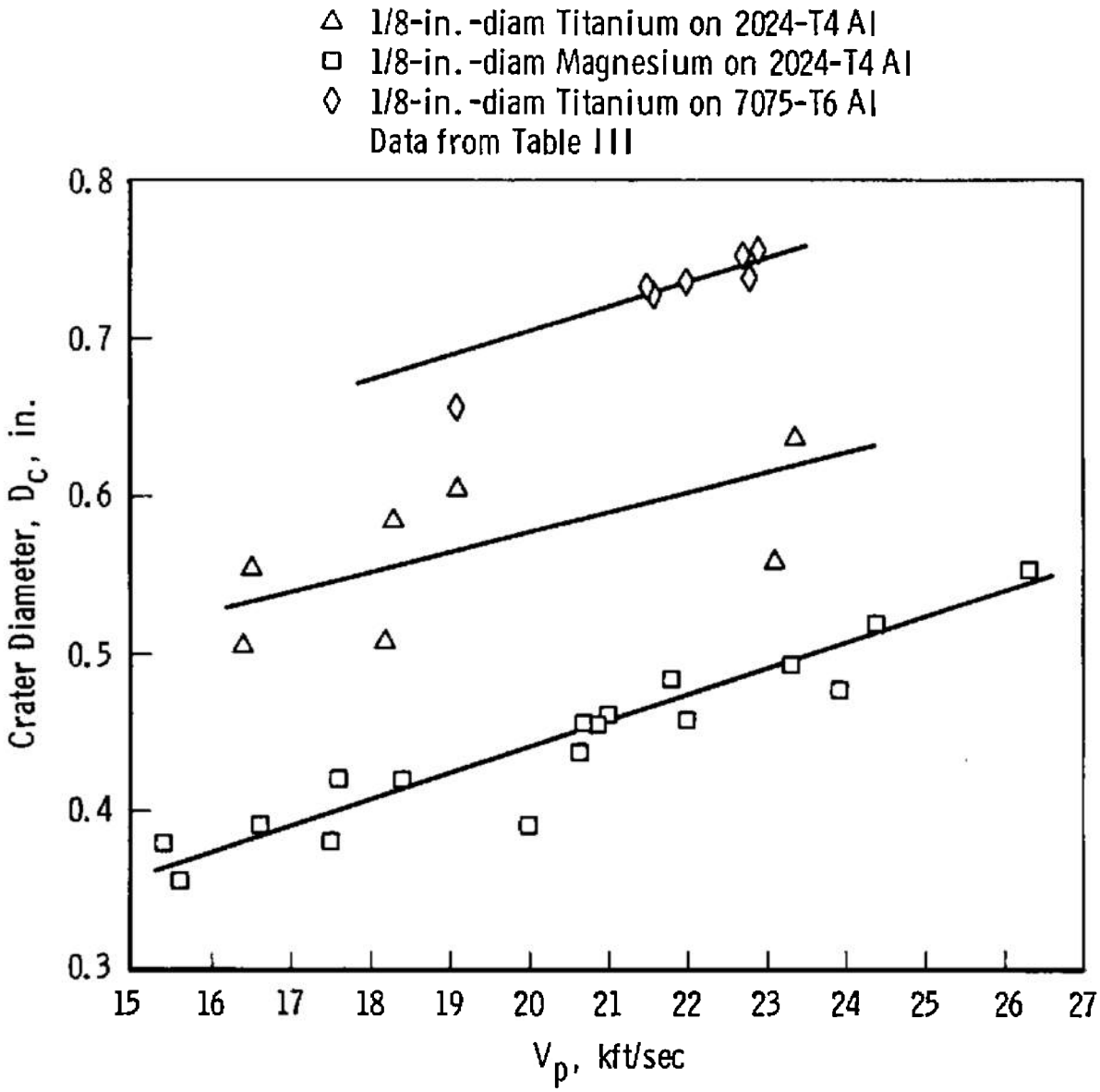

Fig. 11 Crater Diameter versus Projectile Velocity

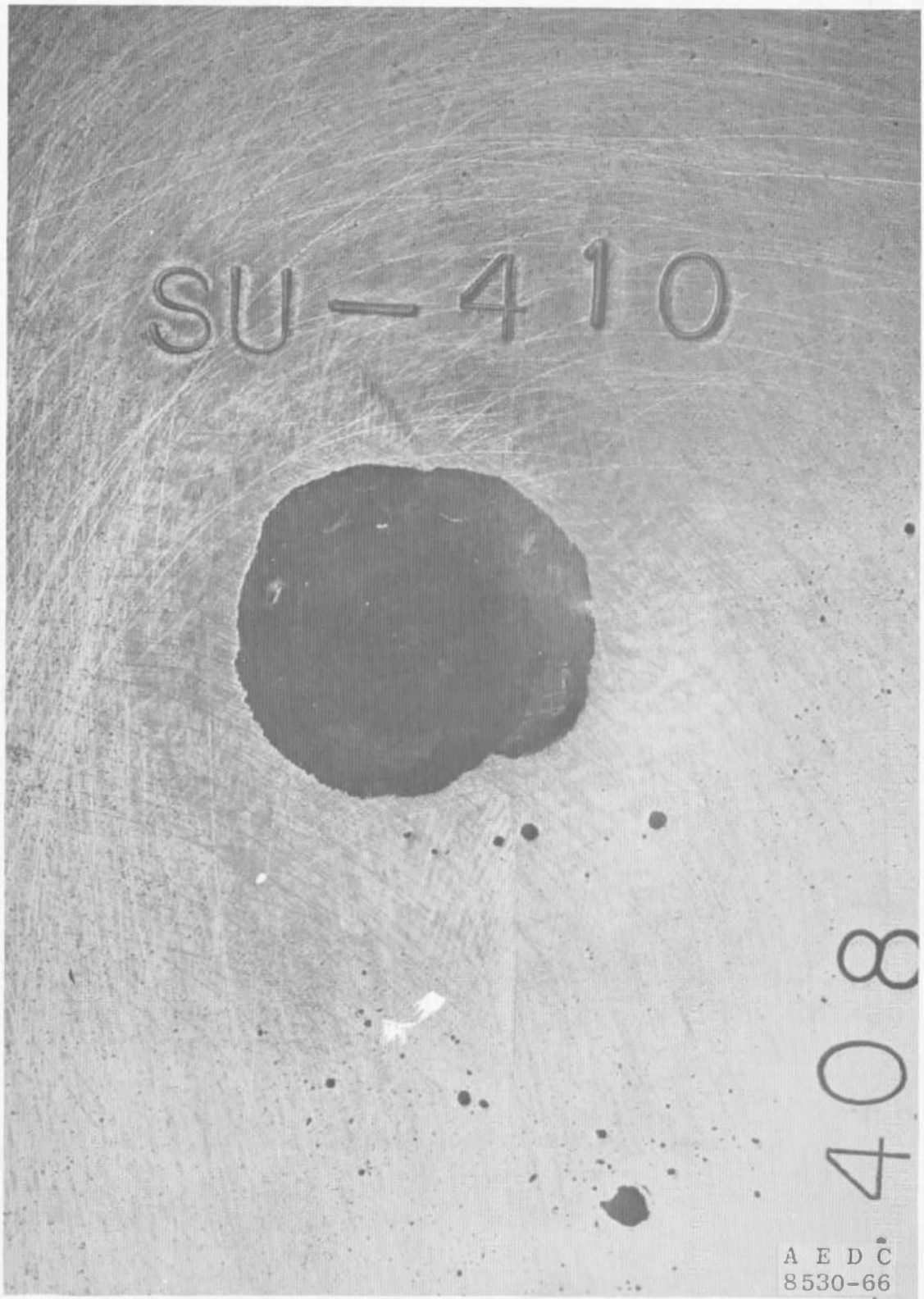

Fig. 12 Photograph of Milled Target Surface – 7075-T6 Al

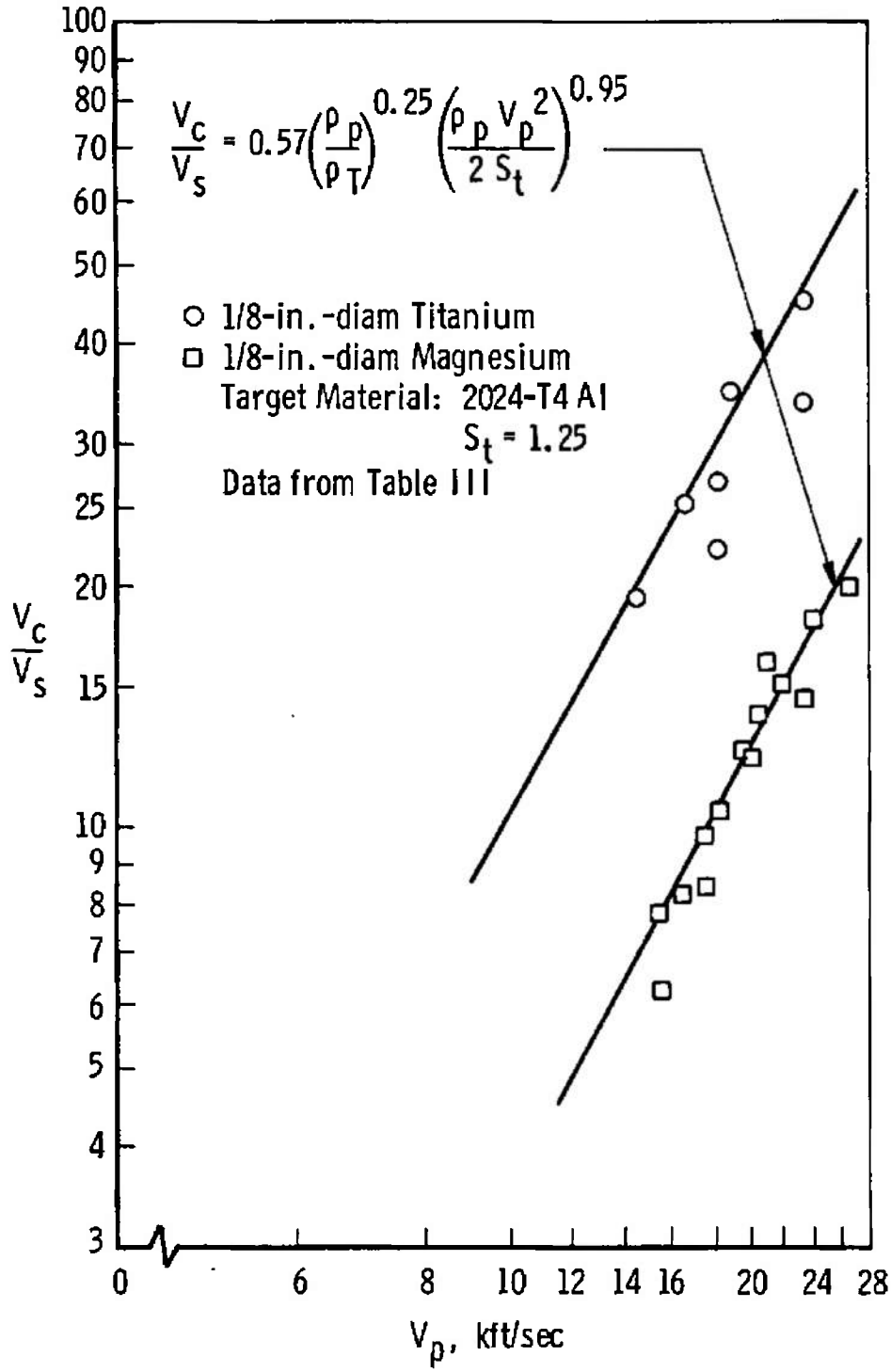

Fig. 13 Dimensionless Crater Volume versus Projectile Velocity for 2024-T4 Al Targets

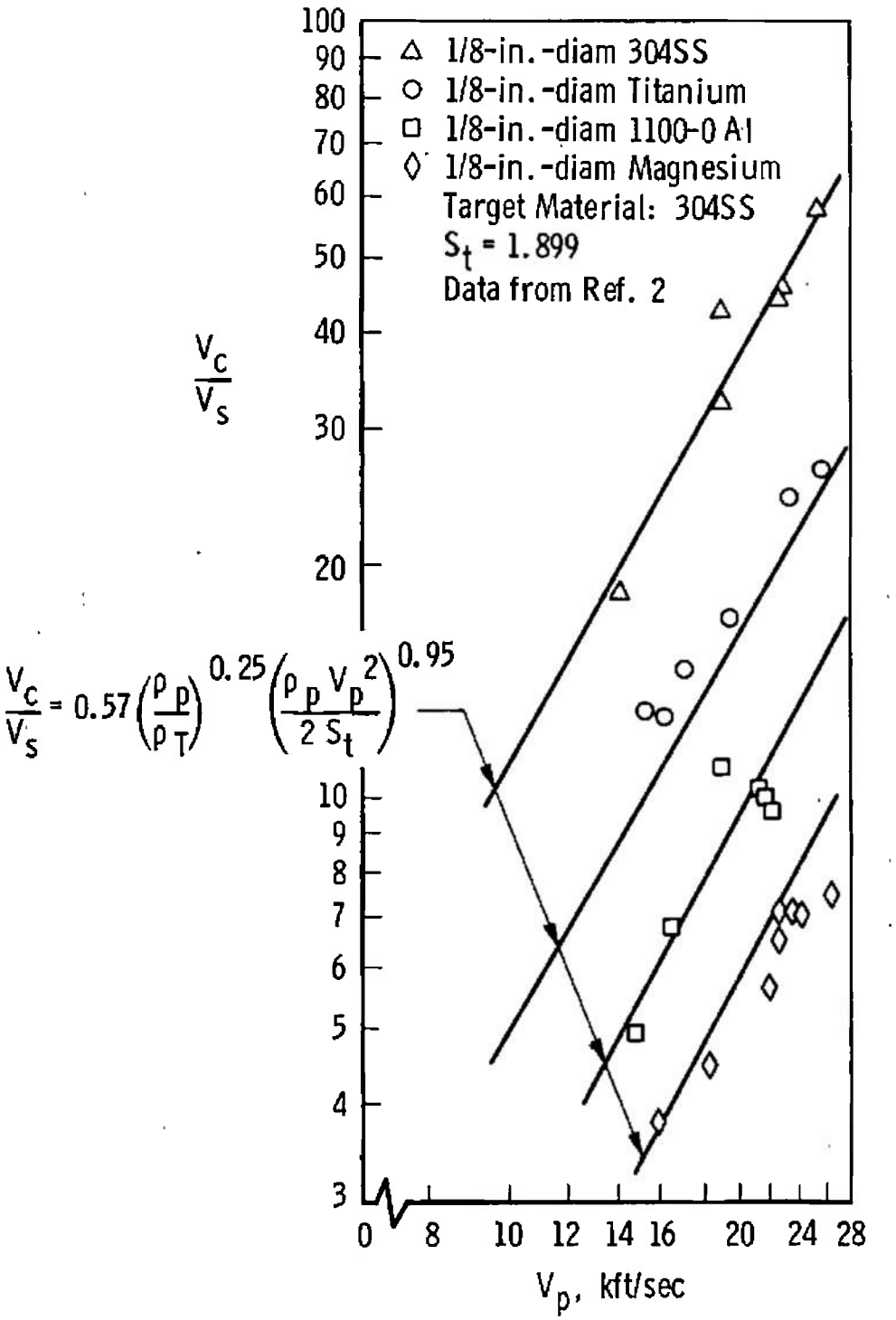

Fig. 14 Dimensionless Crater Volume versus Projectile Velocity for 304SS Targets

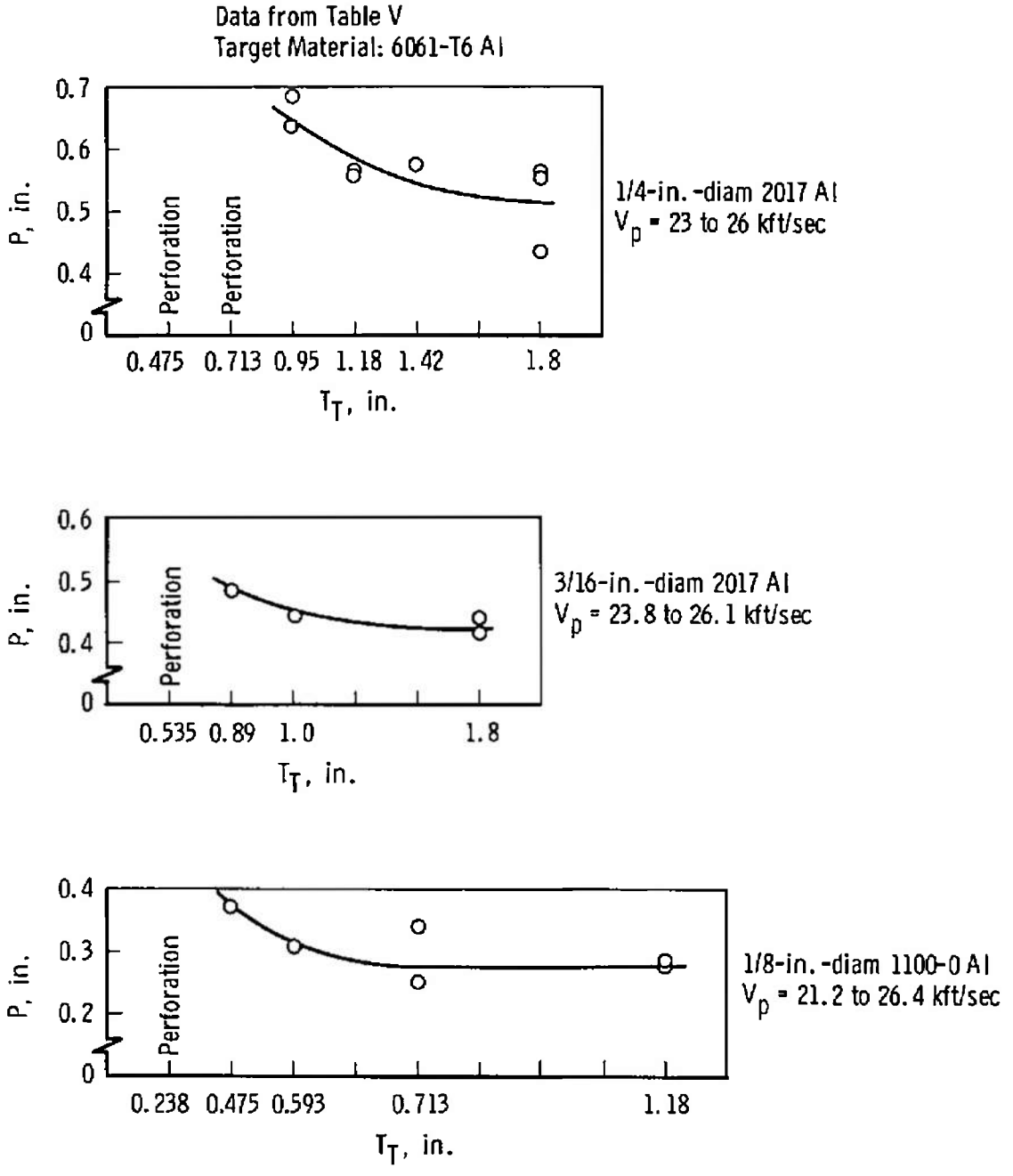

Fig. 15 Penetration versus Target Thickness

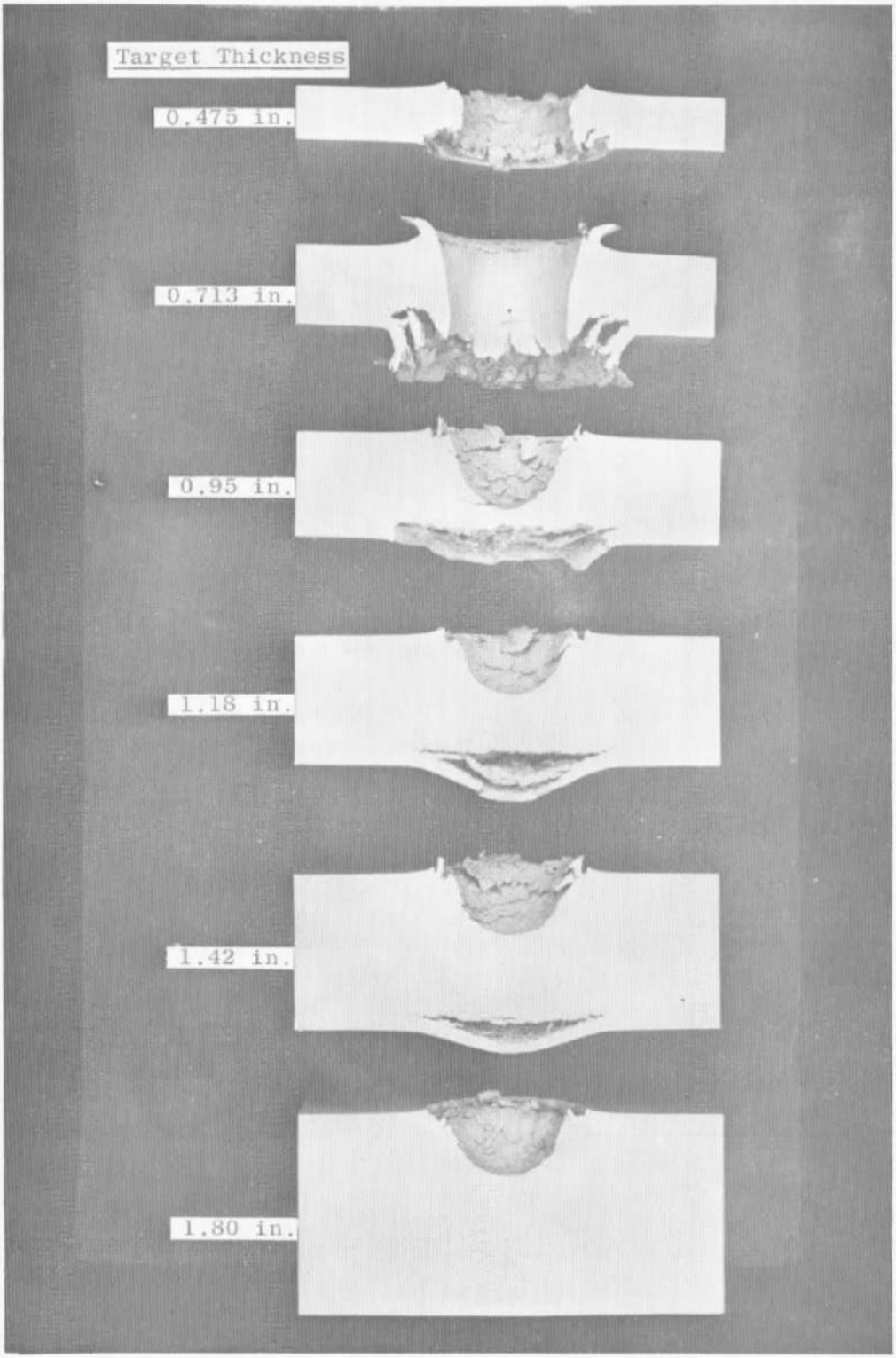

Fig. 16 Typical Damage Resulting from 1/4-in.-diam Al Sphere Impacts

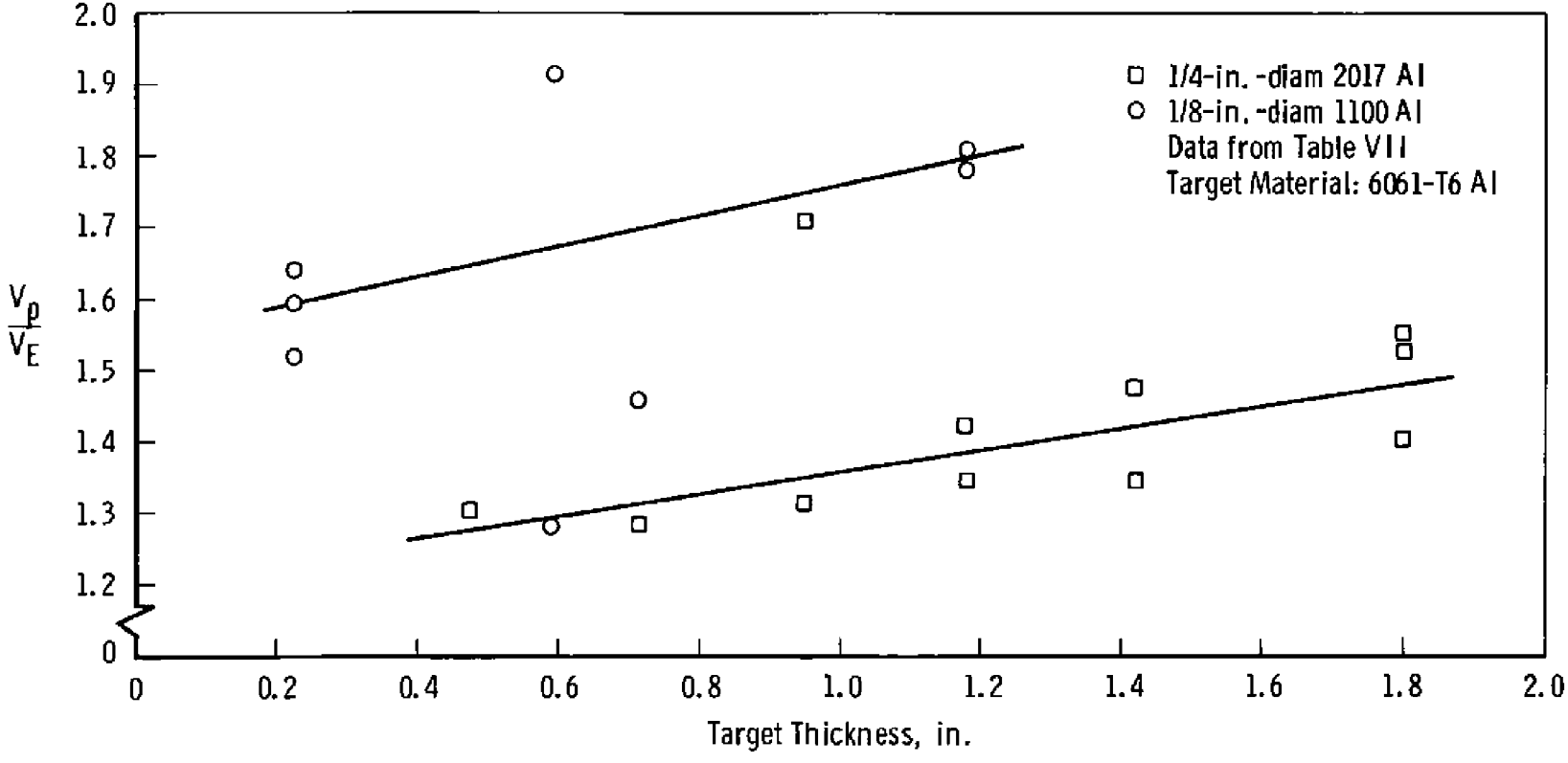

Fig. 17 Projectile Velocity/Ejecta Velocity versus Target Thickness

TABLE I
RESULTS OF PEGASUS FIRINGS – 1/16-IN.-DIAMETER PROJECTILES

Shot No.	Projectile Material	Projectile Velocity, fps	Output Voltage, v	Hole Diameter, in.	Range Pressure, mm Hg
132	Al 2017	15,200	20	0.115	10
133	↓	16,300	20	0.120	↓
135		20,500	20	0.137	
136		19,600	9	0.129	
137		21,300	6	0.140	
144		12,100	**	0.107	
145		22,100	12	0.124	
148		19,000*	10	0.123	
150		21,900	8	0.130	
151		20,800	20	0.128	
152		21,300	31	0.129	
153		22,500	20	0.135	
154		24,200	30	0.125	
158		19,800*	44	0.123	
167		26,500	30	Not Available	
140	Lexan®	17,200	40	0.129	1
155	Al 2017	27,000*	30	0.126	↓
157	↓	27,200	32	0.143	
161		15,600	24	0.117	
162		17,800	20	Not Available	
163		18,800	20	↓	
165		22,400	16		
166		23,100	36		

*Velocity Determined Using the Aluminized Plastic Film, All Others by High-Speed Framing Camera.

**Oscilloscope Traces Overexposed.

TABLE II
RESULTS OF SATURN TARGET CONFIGURATION FIRINGS – 1100-0 ALUMINUM PROJECTILES

a. Wall Results

Shot No.	Projectile Diameter, in.	Projectile Velocity, fps	Front Plate Thickness, in.	Remarks
SU-377	1/16	16,400	0.117	No Perforation
379	1/16	12,900	↓	No Perforation
380	1/16	23,800	↓	No Perforation
381	1/8	17,500	↓	Rear of Target Face Split

b. Tank Results

Shot No.	Projectile Diameter, in.	Projectile Velocity, fps	Tank Pressure, psia	Tank Atmosphere	Front Plate Thickness, in.	Remarks
SU-456	1/8	14,700	15	O_2	0.063	No Foam on Either Target - Target Perforated - No Burning
458	↓	22,500*	15	↓	↓	
459	↓	14,800	7	↓	↓	Perforation and Burning
460	↓	14,300	15	↓	↓	
461	↓	27,800	5	↓	↓	
463	↓	24,800*	1 atm	air	↓	
464	↓	27,100	↓	↓	↓	
465	↓	19,800	↓	↓	↓	
466	↓	15,300	↓	↓	↓	
470	↓	23,400	5	N_2	↓	
471	↓	22,300*	5	O_2	↓	
472	↓	20,600	7	50 percent O_2 50 percent N_2	↓	Plexiglas® Rear Face - Perforation and Burning
473	↓	20,900	7	50 percent O_2 50 percent N_2	0.125	
474	↓	18,300	3.5	O_2	↓	
475	↓	24,600	5	↓	↓	Plexiglas® Rear Face - Perforation and Burning - D-65 Overcoat
476	↓	18,800	↓	↓	↓	Plexiglas® Rear Face - Perforation and Burning - KEL F-800 Overcoat
477	↓	22,100	↓	↓	↓	Plexiglas® Rear Face - Perforation and Burning - Two Tanks Bolted Together - D-65 Overcoat
478	↓	20,000	↓	↓	↓	Plexiglas® Rear Face - Perforation and Burning - Two Tanks Bolted Together - Black Insulation Overcoat

All Firings at 1 mm Hg Range Pressure

*Velocities Determined Using the Aluminized Plastic Film, All Others by High-Speed Framing Camera.

TABLE III
VELOCITY AND CRATER DATA FOR IMPACTS INTO SEMI-INFINITE TARGETS BY 1/8-IN.-DIAMETER PROJECTILES

Shot No.	Projectile Material	Projectile Velocity, fps	Target Material	Crater Diameter, in.	Crater Depth, in.	Crater Volume, $in.^3$	P/d_p	Percent Variation between Actual and Predicted P/d_p	Range Pressure, mm Hg
368	T_i	16,500*	2024-T4 Al	0.558	0.268	0.0260	2.14	-2.33	1.0×10^{-3}
369		18,300*		0.585	0.279	0.0274	2.23	+0.44	3.0×10^{-4}
370		18,200*		0.507	0.259	0.0229	2.07	+7.70	4.5×10^{-4}
372		23,400*		0.635	0.306	0.0475	2.45	+8.16	5.1×10^{-4}
373		19,100*		0.606	0.284	0.0361	2.27	+1.76	6.7×10^{-4}
374		23,100*		0.558	0.322	0.0350	2.57	+1.94	4.1×10^{-4}
375		14,300*		0.421	0.241	0.0195	2.01	-5.47	3.0×10^{-4}
390		16,400*		0.507	0.279	0.0291	2.23	-5.83	6.0×10^{-4}
417	Mg	16,600		0.391	0.136	0.0085	1.09	+2.75	1
418		17,600		0.421	0.143	0.01001	1.145	+3.05	
419		20,800*		0.456	0.163	0.0141	1.305	0	
420		21,000*		0.462	0.170	0.0167	1.36	-3.67	
421		24,400		0.5195	0.189	0.0189	1.51	-3.97	
422		21,800		0.483	0.170	0.0155	1.36	-1.47	
424		23,900		0.476	0.183	0.0188	1.465	-1.70	
425		18,400		0.421	0.144	0.0107	1.15	+4.34	
426		20,700		0.456	0.160	0.0078	1.28	+1.56	
428		15,600		0.358	0.139	0.0064	1.11	-2.70	
429		23,300		0.494	0.175	0.0148	1.40	0	
446		15,400		0.383	0.141	0.0081	1.13	-5.31	
447		26,300		0.553	0.191	0.0205	1.53	0	
448		20,600		0.436	0.167	0.0127	1.335	-2.62	
449		22,000		0.456	0.166	0.0158	1.33	+1.50	
450		17,500		0.383	0.140	0.0086	1.12	+3.57	
451		20,000		0.391	0.155	0.0128	1.24	+2.41	
432	1100-0 Al	13,200**		0.383	0.162	0.0109	1.295	-1.15	
433		17,500**		0.483	0.194	0.0183	1.55	0	
434		21,200**		0.558	0.222	0.0282	1.785	-1.40	5
435		22,600**		0.575	0.231	0.0297	1.85	-0.54	
436		20,400		0.548	0.219	0.0259	1.75	-1.71	
437		16,800		0.489	0.190	0.01697	1.52	-2.63	
438		19,400		0.489	0.209	0.02197	1.675	-3.07	
439		18,100		0.489	0.204	0.01898	1.63	-2.09	10
440		21,900		0.575	0.230	0.0306	1.84	-2.17	10
393	T_i	19,100	7075-T6 Al	0.664	0.277	0.0405	2.22	+2.25	10
406		12,900*		0.313	0.233	0.0126	1.86	-5.91	6.0×10^{-4}
407		15,900*		0.524	0.296	0.0315	2.37	-13.92	5.2×10^{-4}
408		21,500*		0.767	0.302	0.057	2.41	+2.08	4.8×10^{-4}
409		21,600*		0.759	0.305	0.055	2.44	+1.22	5.5×10^{-4}
410		22,700*		0.806	0.308	0.0617	2.46	+3.68	5.3×10^{-4}
411		22,800*		0.774	0.320	0.0654	2.56	0	4.5×10^{-4}
412		22,900*		0.813	0.316	0.0691	2.53	+1.18	5.8×10^{-4}
413		22,000*		0.774	0.313	0.0577	2.50	+0.40	5.9×10^{-4}
403		22,100*	6061-T6 Al	0.717	0.361	0.0632	2.89	-13.14	6.4×10^{-4}
442	Mg	16,900		0.376	0.160	0.0112	1.28	-12.50	1
443		18,900		0.414	0.174	0.0138	1.39	-18.70	0.15
444		11,300**		0.271	0.118	0.0059	0.944	-9.32	5
452		22,400		0.483	0.172	0.0171	1.379	-2.14	1
281	1100-0 Al	22,500		0.485	0.239	0.066	1.91	-5.75	1
441		13,800		0.376	0.184	0.0132	1.47	-14.42	5
445		13,800		0.271	0.131	0.0071	1.05	+23.81	5
453		11,000		0.293	0.108	0.00472	0.863	+29.77	1

*Corrected Aluminized Plastic Film Velocities (See Text).

**Velocities Determined Using Aluminized Plastic Film - No Correction Needed.

TABLE IV
VELOCITY AND CRATER DATA FOR IMPACTS INTO 1100-0 ALUMINUM BY 1/8-IN.-DIAMETER PROJECTILES

Shot No.	Projectile Material	Projectile Velocity, fps	Crater Diameter, in.	Crater Depth, in.	Crater Volume, in.^{3}	P/d_p	Range Pressure, mm Hg
T-1016	1100-0 Al	30,300*	0.726	0.393	0.1083	3.14	0.10
-1017	↓	24,100	0.6942	0.358	0.0851	2.87	↓
-1018	↓	21,400	0.641	0.331	0.0734	2.64	1
-1019	↓	27,600	0.709	0.391	0.094	3.13	↓
-1020	↓	25,800	0.696	0.380	0.088	3.04	3
-1021	↓	26,300	0.694	0.372	0.086	2.98	↓
-1024	↓	27,300	0.709	0.386	0.094	3.08	↓
-1025	↓	28,100	0.715	0.395	0.103	3.16	↓
-1037	P_b	13,700	0.701	0.650	0.1910	5.2	10
-1038	↓	15,000	0.734	0.689	0.2099	5.5	↓
-1039	↓	16,700	0.754	0.762	0.2722	6.1	↓
-1041	↓	15,600	0.707	0.755	0.2337	6.04	↓
-1042	↓	21,100	0.861	0.813	0.3298	6.5	↓

*Velocity Determined Using Aluminized Plastic Film, All Others by Framing Camera.

TABLE V
VELOCITY AND CRATER DATA FOR IMPACTS INTO FINITE TARGETS OF 6061-T6 ALUMINUM

Shot No.	Projectile Diameter, in.	Projectile Material	Target Thickness, in.	Projectile Velocity, fps	Crater Volume, in.^{3}	Crater Diameter, in.	Crater Depth, in.	Range Pressure, mm Hg
SU-300	1/16	1100-0 Al	0.12	21,400*	---	0.22**	---	2
353	↓	↓	0.12	20,800	---	0.212**	---	↓
354			0.178	23,500	---	0.153**	---	
356			0.296	24,300	0.0043	0.244	0.139	
302	1/8		0.238	21,200	---	0.436**	---	1
303			0.475	23,200	0.0433	0.5226	0.310	
305			0.475	21,000	0.0360	0.506	0.277	
306			0.593	26,400	0.0854	0.676	0.373	
308			0.713	25,400	0.0714	0.666	0.342	
311			1.18	25,700	0.0452	0.569	0.287	
313			0.238	25,600	---	0.479**	---	
339			0.593	18,800	0.0293	0.412	0.233	
340			1.18	24,800	0.0460	0.5203	0.277	
341			0.713	21,200	0.0337	0.5035	0.250	
346			1.18	25,500	0.0446	0.5183	0.274	
350			0.238	26,000	---	0.488**	---	
351			0.475	22,000	0.0365	0.5062	0.292	
315	3/16	2017 Al	0.535	25,400	---	0.838**	---	
316			0.713	24,700	---	0.903**	---	
317			0.89	26,100	0.180	0.874	0.488	
318			1.00	25,700	0.168	0.884	0.447	
321			1.80	25,600	0.151	0.854	0.440	
334			1.80	23,800	0.1336	0.8477	0.415	
358			0.713	18,900	0.1619	0.8831	0.530	
455***			0.89	22,900	0.2554	0.8955	0.548	
322	1/4		0.475	23,800	---	0.926**	---	
323			0.713	25,300	---	1.124**	---	
324			0.95	25,300	0.381	1.107	0.686	
325			1.18	22,900	0.321	1.146	0.549	
327			1.8	25,300	0.345	1.130	0.562	
328			1.42	24,600	0.343	1.068	0.576	
329			1.18	23,200*	0.3003	1.068	0.559	
330			1.42	24,800*	0.328	1.191	0.568	
331			1.8	25,600	0.3833	1.407	0.572	
333			1.8	25,100	0.1507	0.8549	0.433	
335			0.713	25,300	---	0.818**	---	
336	↓	↓	0.95	23,400	0.347	1.092	0.639	↓

*Velocity Determined Using Aluminized Plastic Film, All Others by Framing Camera.

**Target Perforated, Only Diameter Data Available.

***Target Under 80,000-psi Stress.

TABLE VI
TERMINAL EFFECTS OF FINITE TARGET IMPACTS

Shot No.	Projectile Velocity, fps	T_T/P	Projectile Diameter, in.	Remarks
SU-300	21,400	---	1/16	Target Perforated
353	20,800	---	1/16	Target Perforated
354	23,500	---	1/16	Target Perforated
356	24,300	1.20	1/16	Rear Surface Deformation
302	21,200	---	1/8	Target Perforated
303	23,200	1.53		Rear Surface Spallation
305	21,200	1 72		Rear Surface Spallation
306	26,400	1.59		Rear Surface Spallation
308	25,400	2.08		Rear Surface Deformation
311	25,700	4.12		No Rear Surface Effects
313	25,600	---		Target Perforated
339	18,800	2.54		Very Slight Rear Surface Deformation
340	24,800	4.26		No Rear Surface Effects
341	21,200	2.85		Extremely Slight Rear Surface Deformation
346	25,500	4.31		No Rear Surface Effects
350	25,000	---		Target Perforated
351	22,000	1.625		Rear Surface Spallation
315	25,400	---	3/16	Target Perforated
316	24,700	---		Target Perforated
317	26,100	1.83		Rear Surface Spallation
318	25,700	2.24		Rear Surface Deformation
321	25,600	4.1		No Rear Surface Effects
334	23,800	4.34		No Rear Surface Effects
358	18,900	1.35		Rear Surface Spallation
322	23,800	---	1/4	Target Perforation
323	25,300	---		Target Perforation
324	25,300	1.38		Rear Surface Spallation
325	22,900	2.15		Rear Surface Deformation
327	25,300	3.2		Very Slight Rear Surface Deformation
328	24,600	2.47		Slight Rear Surface Deformation
329	23,200	2 12		Rear Surface Deformation
330	24,800	2.5		Slight Rear Surface Deformation
331	25,600	3.15		Very Slight Rear Surface Deformation
333	25,100	4.16		Very Slight Rear Surface Deformation
335	25,300	---		Target Perforation
336	23,400	1.49		Rear Surface Spallation

TABLE VII
SPALL VELOCITIES

Shot No.	Projectile Velocity, fps	Target Thickness, in.	Ejecta Velocity, fps	Projectile Diameter, in.	V_p/V_E
SU-306	26,400	0.593	13,800	1/8	1.915
313	25,600	0.238	15,600	1/8	1.640
316	24,700	0.713	15,000	3/16	1.640
317	26,100	0.890	16,300	3/16	1.605
318	25,700	1.000	16,800	3/16	1.470
322	23,800	0.475	18,200	1/4	1.305
324	25,300	0.950	14,800	↓	1.710
325	22,900	1.180	16,100	↓	1.420
326	25,100	0.142	17,000	↓	1.475
327	25,300	1.800	18,100	↓	1.400
329	23,800	1.180	17,700	↓	1.345
330	25,600	1.420	19,000	↓	1.345
331	25,600	1.800	16,800	↓	1.525
333	25,100	1.800	16,200	↓	1.550
334	23,800	1.800	16,800	3/16	1.415
335	25,300	0.713	19,800	1/4	1.280
336	23,400	0.950	17,800	1/4	1.315
339	18,800	0.593	14,700	1/8	1.280
340	24,800	1.180	13,700	↓	1.810
341	21,200	0.713	14,500	↓	1.460
346	25,500	1.180	14,400	↓	1.780
350	26,000	0.238	16,300	↓	1.595
351	22,000	0.238	14,500	↓	1.520
353	20,800	0.120	16,700	1/16	1.250

TABLE VIII
MISCELLANEOUS LAUNCHINGS

Shot No.	Projectile Material	Target Material	Projectile Velocity, fps	Projectile Diameter, in.
SU-278	Al 2017	Norbide	21, 600	1/16
279	Lexan®	↓	5, 800	0. 300 (0.305 long)
280	Al 2017	↓	23, 800	1/8
382	Dylite®	Al 1100	14, 700	1/8
383	↓	↓	11, 100	↓
384			11, 300	
386			11, 600	
388			10, 200	
392			6, 600	
394			7, 200	
395			6, 200	
399			7, 200	
400			6, 800	
401			6, 800	
402			7, 000	

Norbide (6 x 6 x 1/2 in.) - Boron Nitrite

APPENDIX I
VKF HYPERVELOCITY IMPACT RANGE S-1

RANGE DESCRIPTION

Hypervelocity Impact Range S-1 is shown in Fig. I-1. In addition to the two-stage, light-gas launcher, which accelerates the impact projectile to the desired test velocity, the range comprises: (1) a blast chamber, into which muzzle gases expand and in which the projectile is separated from the sabot which adapts it to the bore of the launch tube; (2) a connecting tube; and (3) the target chamber, where the test specimen is impacted by the projectile. Range pressures can be adjusted to any value between atmospheric and 10^{-6} mm Hg. The major dimensions of the range and of the launcher appear in Table I-1.

INSTRUMENTATION

Pressure

Range pressures down to 10^{-3} mm Hg are measured using thermocouple-type transducers. Ionization gages serve at the lower pressures. Range and target chamber pressures are monitored continuously. Pressure measurement systems are periodically calibrated against McLeod gages.

VKF HYPERVELOCITY IMPACT RANGE S-2

RANGE DESCRIPTION

Hypervelocity Impact Range S-2 is shown in Fig. I-2. In addition to the two-stage, light-gas launcher, which accelerates the impact projectile to the desired test velocity, the range comprises: (1) a blast chamber, into which muzzle gases expand and in which the projectile is separated from the sabot which adapts it to the bore of the launch tube; (2) a connecting tube; and (3) the target chamber, where the test specimen is impacted by the projectile. Range pressure can be adjusted to any value between atmospheric and 10^{-6} mm Hg. The major dimensions of the range and launcher appear in Table I-2. As is also indicated in Table I-2, preheating and cooling of target specimens is possible over the temperature range from -200 to 1500°F. Target temperature is remotely controlled while altitude simulation is maintained. Targets can also be stressed to a total load of 100,000 lb along either or both of two perpendicular axes during heating (or cooling) and impact testing.

INSTRUMENTATION

Pressure

These systems are identical to those previously described for range S-1.

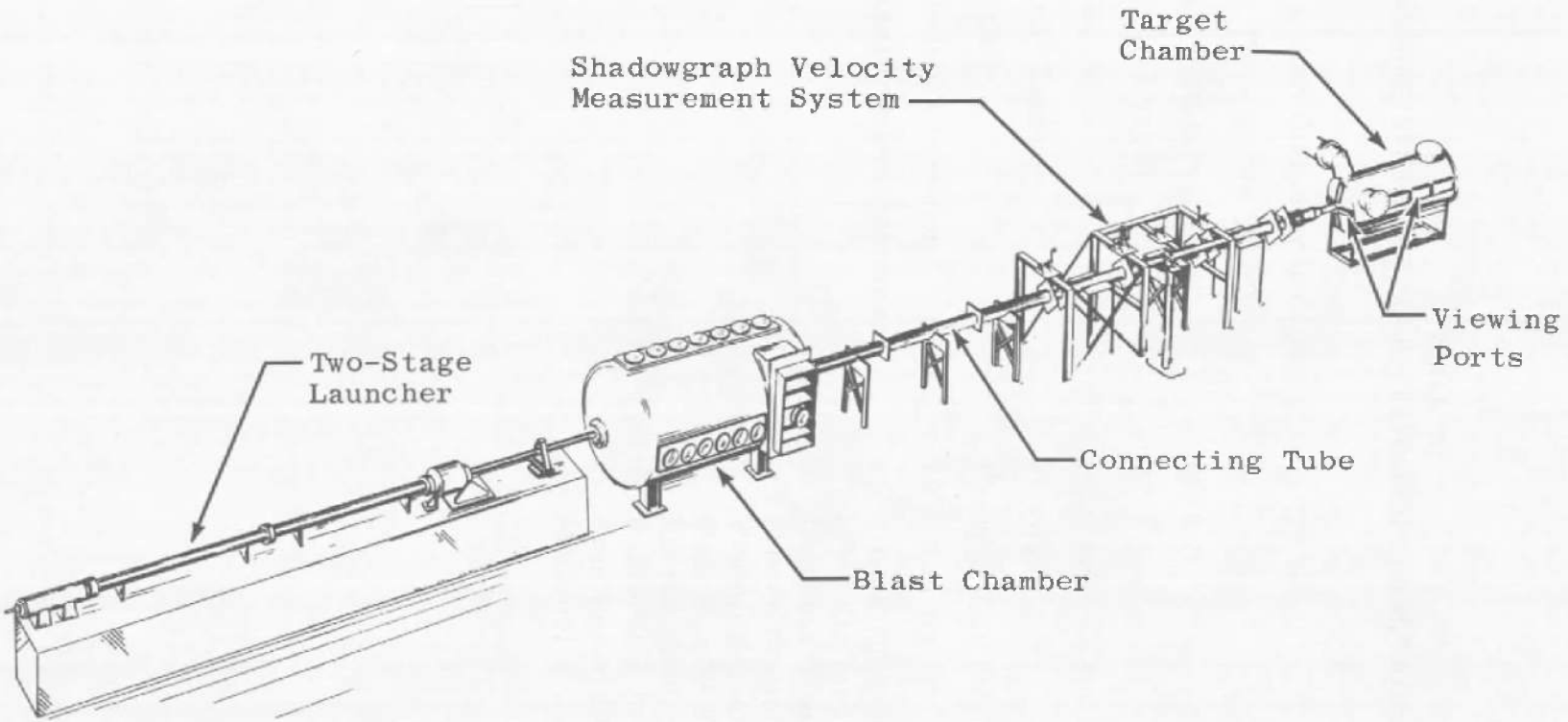

Fig. I-1 VKF Hypervelocity Impact Range S-1 Components

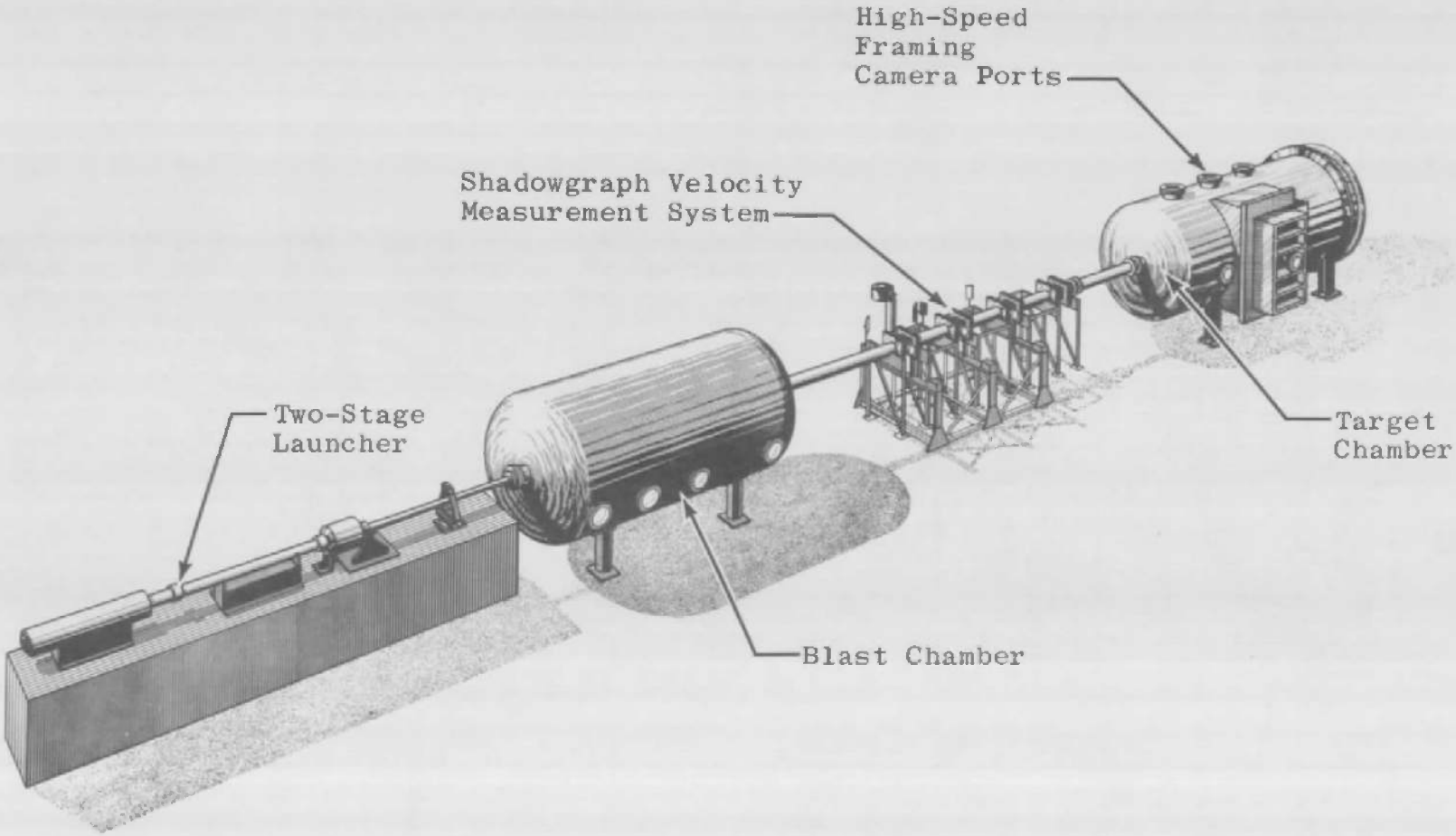

Fig. I-2 VKF Hypervelocity Impact Range S-2 Components

TABLE I-1
CHARACTERISTICS OF VKF HYPERVELOCITY IMPACT RANGE S-1

Target Chamber Diameter/Length	2.5/7 ft
Connecting Tube Inside Diameter	8 in.
Blast Tank, Diameter/Length	6/15 ft
Overall Range Length	87.5 ft
Launch Tube Bore	0.30 or 0.50 in.
Initial Energy Source	Powder
Propellant Gas	Hydrogen or helium
Minimum Range Pressure	10^{-6} mm Hg
Velocity Measurement Systems:	a. Streak Cine-Shadowgraph (Two Stations) b. Discrete-Frame Shadowgraph (Three Stations) c. Framing Camera (One Station - 80 Frames - Max Frame Rate: 1.4×10^{6}/sec) d. Perforable Screens of Aluminized Plastic Film (Two Stations)

TABLE I-2
CHARACTERISTICS OF VKF HYPERVELOCITY IMPACT RANGE S-2

Target Chamber Diameter/Length	6/21 ft
Connecting Tube Inside Diameter	8 in.
Blast Tank, Diameter/Length	6/15 ft
Overall Range Length	101 ft
Launch Tube Bore	0.30 or 0.50 in.
Initial Energy Source	Powder
Propellant Gas	Hydrogen or helium
Minimum Range Pressure	10^{-6} mm Hg
Target Preheat Capability	1500°F
Target Precool Capability	-200°F
Target Stress Capability	100,000-lb Tension along Either or Both of Two Axes
Velocity Measurement Systems:	a. Streak Cine-Shadowgraph (Two Stations) b. Discrete-Frame Shadowgraph (Three Stations) c. Framing Camera (One Station - 80 Frames - Max Frame Rate: 1.4×10^6/sec) d. Perforable Screens of Aluminized Plastic Film (Two Stations)

UNCLASSIFIED

Security Classification

DOCUMENT CONTROL DATA - R&D

(Security classification of title, body of abstract and indexing annotation must be entered when the overall report is classified)

1 ORIGINATING ACTIVITY (Corporate author)
Arnold Engineering Development Center
ARO, Inc., Operating Contractor
Arnold Air Force Station, Tennessee

2a REPORT SECURITY CLASSIFICATION
UNCLASSIFIED

2b GROUP
N/A

3 REPORT TITLE
SUMMARY OF IMPACT TESTING FOR NASA PROJECT SUPER

4 DESCRIPTIVE NOTES (Type of report and inclusive dates)
N/A

5 AUTHOR(S) (Last name, first name, initial)
Payne, J. J., ARO, Inc.

6 REPORT DATE	7a TOTAL NO OF PAGES	7b NO OF REFS
September 1966	56	9

8a CONTRACT OR GRANT NO
AF 40(600)-1200

b PROJECT NO 9514

c System 920E

d

9a ORIGINATOR'S REPORT NUMBER(S)
AEDC-TR-66-97

9b OTHER REPORT NO(S) (Any other numbers that may be assigned this report)
N/A

10 AVAILABILITY/LIMITATION NOTICES
Qualified users may obtain copies of this report from DDC.

11 SUPPLEMENTARY NOTES
N/A

12 SPONSORING MILITARY ACTIVITY
National Aeronautics and Space Administration, Marshall Space Flight Center, Huntsville, Alabama

13 ABSTRACT

Hypervelocity impact tests were performed using Pegasus detector panels, simulated Saturn fuel tanks, and finite and semi-infinite targets. The impact velocity and crater parameters, where applicable, are given. It was determined that the output voltage of the Pegasus detector panels was not a function of projectile velocity nor of ambient pressure. The simulated Saturn fuel tanks showed evidence of burning after having been perforated by the projectile. The semi-infinite targets tested were 2024-T4, 6061-T6, and 7075-T6 Aluminum. Penetration data are presented for impact velocities from 11,000 to 30,300 fps and are used to determine values of target deformation stress. The correlation between the penetration data and an empirical relation using these stress values is approximately within ±2.5 percent. An empirical relationship to aid in crater volume prediction is presented. The results of the finite target work indicate that, to ensure that spall is not formed, the target thickness should be approximately 2.5 times the crater depth in a semi-infinite target. (U)

DD FORM 1 JAN 64 1473

UNCLASSIFIED

Security Classification

UNCLASSIFIED

Security Classification

14 KEY WORDS	LINK A		LINK B		LINK C	
	ROLE	WT	ROLE	WT	ROLE	WT
1 Project SUPER						
2 extraterrestrial research						
3 impact ~~testing~~ ing						
4 hypervelocity impacting						
5 PEGASUS						
~~SATURN~~						
1 - 2						

INSTRUCTIONS

1. ORIGINATING ACTIVITY: Enter the name and address of the contractor, subcontractor, grantee, Department of Defense activity or other organization *(corporate author)* issuing the report.

2a. REPORT SECURITY CLASSIFICATION: Enter the overall security classification of the report. Indicate whether "Restricted Data" is included. Marking is to be in accordance with appropriate security regulations.

2b. GROUP: Automatic downgrading is specified in DoD Directive 5200.10 and Armed Forces Industrial Manual. Enter the group number. Also, when applicable, show that optional markings have been used for Group 3 and Group 4 as authorized

3. REPORT TITLE: Enter the complete report title in all capital letters. Titles in all cases should be unclassified. If a meaningful title cannot be selected without classification, show title classification in all capitals in parenthesis immediately following the title.

4. DESCRIPTIVE NOTES: If appropriate, enter the type of report, e.g., interim, progress, summary, annual, or final. Give the inclusive dates when a specific reporting period is covered.

5. AUTHOR(S): Enter the name(s) of author(s) as shown on or in the report. Enter last name, first name, middle initial. If military, show rank and branch of service. The name of the principal author is an absolute minimum requirement.

6. REPORT DATE: Enter the date of the report as day, month, year, or month, year. If more than one date appears on the report, use date of publication.

7a. TOTAL NUMBER OF PAGES: The total page count should follow normal pagination procedures, i.e., enter the number of pages containing information.

7b. NUMBER OF REFERENCES: Enter the total number of references cited in the report.

8a. CONTRACT OR GRANT NUMBER: If appropriate, enter the applicable number of the contract or grant under which the report was written.

8b, 8c, & 8d. PROJECT NUMBER: Enter the appropriate military department identification, such as project number, subproject number, system numbers, task number, etc.

9a. ORIGINATOR'S REPORT NUMBER(S): Enter the official report number by which the document will be identified and controlled by the originating activity. This number must be unique to this report.

9b. OTHER REPORT NUMBER(S): If the report has been assigned any other report numbers *(either by the originator or by the sponsor)*, also enter this number(s).

10. AVAILABILITY/LIMITATION NOTICES: Enter any limitations on further dissemination of the report, other than those imposed by security classification, using standard statements such as:

(1) "Qualified requesters may obtain copies of this report from DDC."

(2) "Foreign announcement and dissemination of this report by DDC is not authorized."

(3) "U. S. Government agencies may obtain copies of this report directly from DDC. Other qualified DDC users shall request through _____."

(4) "U. S. military agencies may obtain copies of this report directly from DDC. Other qualified users shall request through _____."

(5) "All distribution of this report is controlled. Qualified DDC users shall request through _____."

If the report has been furnished to the Office of Technical Services, Department of Commerce, for sale to the public, indicate this fact and enter the price, if known.

11. SUPPLEMENTARY NOTES: Use for additional explanatory notes.

12. SPONSORING MILITARY ACTIVITY: Enter the name of the departmental project office or laboratory sponsoring *(paying for)* the research and development. Include address.

13. ABSTRACT: Enter an abstract giving a brief and factual summary of the document indicative of the report, even though it may also appear elsewhere in the body of the technical report. If additional space is required, a continuation sheet shall be attached.

It is highly desirable that the abstract of classified reports be unclassified. Each paragraph of the abstract shall end with an indication of the military security classification of the information in the paragraph, represented as *(TS). (S). (C). or (U)*

There is no limitation on the length of the abstract. However, the suggested length is from 150 to 225 words.

14. KEY WORDS: Key words are technically meaningful terms or short phrases that characterize a report and may be used as index entries for cataloging the report. Key words must be selected so that no security classification is required. Identifiers, such as equipment model designation, trade name, military project code name, geographic location, may be used as key words but will be followed by an indication of technical context. The assignment of links, rules, and weights is optional.

UNCLASSIFIED

Security Classification